A Dynamic Systems Approach to Visual Attention in Infancy

A DISSERTATION SUBMITTED TO THE FACULTY
OF THE UNIVERSITY OF MINNESOTA BY

Robin Sifre

IN PARTIAL FULFILLMENT OF THE
REQUIREMENTS FOR THE DEGREE OF DOCTOR OF
PHILOSOPHY

Advisors: Dr. Jed Elison, Dr. Daniel Berry

June 2021

Acknowledgements

There were many interacting components that gave rise to this complex system. A huge thank you to:

- My advisors, **Jed Elison** and **Dan Berry**, for supporting and being a part of this from the very beginning.
- My committee (**Jed Elison, Dan Berry, Katie Thomas, Eric Feczko**) for providing invaluable feedback.
- Elab members, especially **Sharlotte Irwin** & **Eli Johnson** for helping me wrangle five years of eye-tracking data, **Trevor Day** for assisting with all things resting state, and **Isa Stallworthy** for partnering with me on this adventure through dynamic systems theory.
- **Damian Kelty-Stephen** for helping to herd all the fractal cats.
- My cohort (**Alyssa Palmer, Keira Leneman, Shreya Lakhan-Pal**) for seeing me through the twists and turns of grad school.
- My supportive family, especially **Toby Lubin, Adam Sifre, Emma Sifre,** and **Jesse Sifre**.
- My wonderful partner, **Robert Mitchell**, with whom I was quarantined during my year of dissertating. This wasn't how I imagined my last year of graduate school, and I couldn't have done it without you.

Table of Contents

List of Tables

List of Figures

Introduction

Infants live in a visually cluttered world, and prioritizing attention to meaningful information is arguably the most important challenge they face to efficiently learn about their surroundings. To do so, infants must coordinate multiple attention processes across different timescales.

Coordination is the organization of different parts of a complex system that enable them to effectively work together. Coordination is essential to cognition but has been relatively understudied (Van Orden, et al., 2011). Research on attention is no exception. On the one hand, there is a large body of work documenting the developmental timelines of different attention processes (Amso & Scerif, 2015), and rich theories about how brain development supports their coordination. However, there is a notable lack of research quantifying how these processes become coordinated, as well as a lack of studies that combine both brain imaging data and direct measures of attention. Thus, while we have a clear picture of the developmental timeline of each sub-component of attention, little is known about (a) how these processes become coordinated and (b) how neural development supports their coordination. The primary aim of my dissertation is to expand upon my past work quantifying the processes that make it possible for infants to pay attention in a coordinated way, and to examine how brain development supports these processes.

This dissertation is a two-part study. In **Study 1** I replicate and extend my past work showing age-related increases in eye-gaze fractality in infants by examining

spectrum width (e.g., variability in α). In **Study 2** I present preliminary data on the development of functional brain networks, and a detailed analytic plan of brain-behavior analyses that I will do once the MRI data are finished being processing and cleaned. The team will finish processing the MRI data in the next 1-2 months.

Study 1

Background

The Development of Visual Attention.

Infants live in a visually noisy world, and prioritizing attention to meaningful information is arguably the most important task that they face to efficiently learn about their surroundings (Markant & Amso, 2013). Hierarchical models of attention frame attention as the product of competition (Desimone & Duncan, 1995) or interactions between **bottom-up orienting** (or, exogenously driven responses to physical features of stimuli) and **top-down orienting** (or, endogenously driven, goal-directed attention) (**Error! Not a valid bookmark self-reference.**).

Broadly speaking, these models posit that infants' looking behavior can be understood as an emergent phenomenon that unfolds across development as lower-level attention systems driven by bottom-up stimulus properties catalyze the development of top-down attention processes. As top-down mechanisms develop, they then tune the bottom-up systems, creating a self-organizing feedback loop. This component of the model has been important for understanding early **visual social engagemen**t (Klin, Shultz, & Jones, 2015). Evidence suggests that in addition to specialized cortical regions

for processing social information such as faces, there also exists sub-cortical routes for

social information processing (Johnson, 2005; Lorenzi, Mayer, Rosa-Salva, &

Vallortigara, 2017). Thus, early attentional biases for social stimuli may reflect more

"reflexive" attention pathways and *experience-expectant* development, whereas later-

emerging preferences for social stimuli reflect more volitional pathways shaped by

experience-dependent development. Indeed, human newborns reflexively orient to social

stimuli from birth (Bardi, Regolin, & Simion, 2014; Farroni, Csibra, Simion, & Johnson,

2002; Valenza, Simion, Cassia, & Umiltà, 1996), suggesting that these early attentional

biases may be subcortically mediated. These biases could provide infants with the early

visual experiences with the social world, which in turn tune cortical processing of social

information. Both mechanisms serve to amplify social information in the first years of

life.

From this perspective, early looking behavior is a dynamic phenomenon that

emerges through self-organizational processes across multiple systems and timescales.

Researchers have long recognized the importance of examining the temporal processes of

visual attention development, as it can reveal new information about the relationship

between global average looking times and the processes that give rise to them (e.g.,

Aslin, 2007). Despite this qualitative observation, little work has been done to quantify

the dynamic organization of infants' gaze.
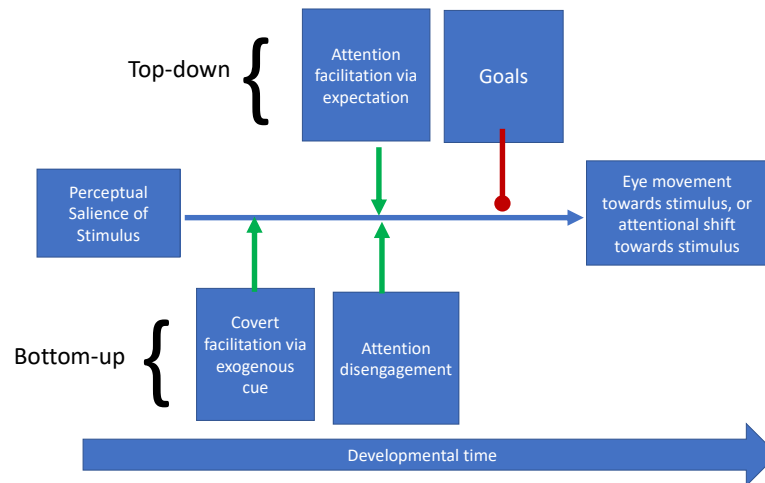
Figure 1. Schmetic of heirarchical models of attention.

Complexity science: A systems-level approach to studying visual attention.

My past work applied methods from Complexity science to quantify the dynamic, self-organizational properties in infants' eye-gaze patterns (Stallworthy et al., 2020). Complexity science is an interdisciplinary field that sits at the intersection of mathematics, computer science, and natural science, and examines complex systems, or systems with many interacting components (Downey, 2012). It encompasses a collection of theories and methods, and there is significant overlap between its core principles and dynamic systems theory (e.g., control parameters, critical states, self-organization, etc.) (Van Orden, Kloos, & Wallot, 2011). It places a strong emphasis on the idea that living and open systems have dynamics that reflect flexible adaptation to their environment, and that behavior is soft-assembled from constraints placed on degrees of freedom by the brain, body, and environment. Thus, task performance can be thought of as a match between an organism's internal constraints and their environment (similar to the arguments laid out by Gibson & Pick, 2000), as well as their ability to flexibly adapt to

changing constraints. Infants' looking behavior, for example, can be thought of as being self-organized through the control parameters put in place by oculomotor and brain maturation, the information present in the environment, as well as attractor states which themselves are shaped by the infant's past experiences and her developmental stage. From this perspective, attention development represents changes in an infant's ability to flexibly adapt and change orienting strategies, or to change her loci of attention when faced with new information.

While these concepts echo principles of self-organization and emergent behavior that have been around for some time, complexity science offers ways to quantify these system dynamics. While multiple methods have been used (e.g. Recurrence Quantification Analysis, ARFIMA models), my dissertation employs Detrended Fluctuation Analysis (DFA) and Multifractal Detrended Fluctuation Analysis (MF-DFA) to measure eye-gaze fractality in infants.

Fractality.

Fractals refer to nested patterns of variability that are *self-similar* across different timescales (Coey, Wallot, Richardson, & Van Orden, 2012a). This self-similarity refers to the idea that the same mathematically-driven pattern can be recursively called at any magnitude to generate a structure comprised of many nested, scale-invariant patterns. Through simple local rules, larger and more complex patterns can emerge.

Mathematically, fractality is the relationship between power (or the amplitude of change) and frequency (how often changes of that amplitude occur) of variation in a time

series (Van Orden et al., 2011). This relationship can be described by the negative slope

(*S*) of the relationship between power (*P(f)*) and frequency (*f*) on a log-log scale, with the

equation *S=P(f)/f* (**Figure 2**). This relationship indicating an inversely proportional

relationship between power and frequency can also be described through power-law

scaling, or the equation P=1/f $^\alpha$. Both the negative slope and α provide a metric of scale-

invariance. When the slope between power and frequency is -1 (α=1), *P(f)* and *f* are

proportional, implying scale-invariance, and self-similarity over nested time scale. This is

referred to as *pink noise* (or 1/f scaling), and is suggestive of a highly-organized system,

that is still flexible to change. It is ubiquitous in nature, (e.g., in mountain ranges and

riverbeds; Mandelbrot, 1982) and human physiology (e.g., BOLD signal at rest; Wink,

Bullmore, Barnes, Bernard, & Suckling, 2008), and may reflect healthy cognitive and

psychobiological systems (Gilden, 2001; Van Orden, Holden, & Turvey, 2003).
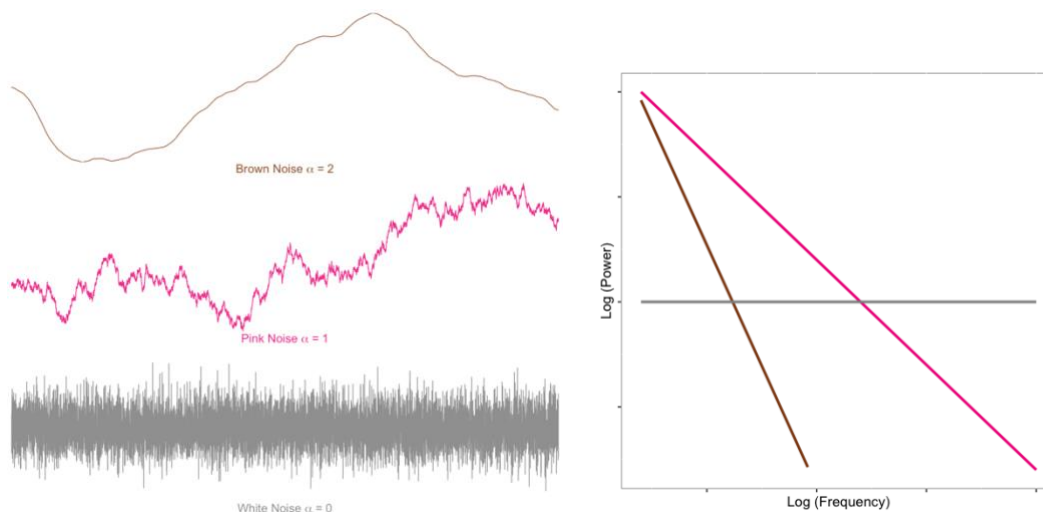
Figure 2. Example of time series with White Noise, Pink Noise, and Brown Noise (left), and their corresponding log(power) vs. log(frequency) plot (right).

Multifractal Systems. Importantly, there are multiple types of interactivity (Ihlen & Vereijken, 2010). The fractal properties described above reflect a type of interactivity called self-organized criticality (SOC; Bak & Chen, 1991) which refers to a system in which many local interactions between sub-components result in emergent global properties (Kelty-Stephen, Palatinus, Saltzman, & Dixon, 2013). For example, schools of fish (Bonabeau & Dagorn, 1995) and ant foraging (Halley & Burd, 2004) are systems that exhibit SOC; the resulting global patterns exhibit fractal properties, but these patterns emerge from local interactions rather than cross-scale interactions. This form of interactivity maps onto theoretical models of visual attention that posit that eye-gaze can be predicted based solely on the physical stimulus saliency (e.g., Itti, Koch & Niebur, 1998). However, hierarchical theories of attention development posit that as bottom-up and top-down processes become more intertwined, interactions do occur between multiple timescales. This multi-scale interactivity occurs when large-scale factors act as contextual constraints upon smaller scale events, and when small-scale factors perturb large-scale factors. A large-scale contextual factor, for example, could be an infants' experience with her mother which make it more likely that she attends to her mother's face relative to a stranger's face with the same low-level stimulus properties. On the other hand, the infant's arousal state – occurring on a smaller timescale – can influence how big of an effect her familiarity with her mother has on the likelihood of her attending to her face

Importantly, both types of interactivity (SOC and multi-scale interactivity) will yield global patterns that can be characterized by a single power-law. This means that

evidence of a single power-law function does not yield information regarding the kind of

interactivity present; it is consistent with interactivity, but not sufficient evidence for one

type or the other (Kelty-Stephen et al., 2013).

One way to determine if a time series exhibits multi-scale interactions is to

examine whether power-law scaling changes over time; if it does, then it is said to be

*multi*fractal. The multifractal spectrum *width* describes how many fractal structures are

needed to describe the time series. If α describes the average relationship between power

and frequency (as described in the *Fractality* section), then MF spectrum width describes

the variance in this structure. More conceptually, the MF spectrum width is thought to

measure the presence of interacting processes across multiple time scales (e.g. rule-

switching behaviors that require the balancing of long-term goals and short-term

feedback; Kelty-Stephen, Stirling, & Lipsitz, 2016).

Fractal Dynamics of Attention.

With the exception of my own work, most evidence of fractal dynamics in eye-gaze

comes from studies on adults. Importantly, variation in eye-gaze data collected from a

fake eye has been shown to yield white noise (Coey, Wallot, Richardson, & Van Orden,

2012b), suggesting that the eye-tracker itself does not produce scale-invariant dynamics.

Relative to the fake eye, data collected from humans fixating on static stimuli do show 1/f

scaling (Coey et al., 2012b). Adults' eye-gaze data is also fractally organized during

visual search tasks, whether searching for the same target repeatedly (Aks, Zelinsky, &

Sprott, 2002), or searching for a target based on a verbal instruction (Stephen, Mirman,

Magnuson, & Dixon, 2009). Because adult eye-gaze data is fractal even during free-viewing (Marlow et al., 2015) and when fixating on static images (Coey et al., 2012b), any argument linking fractal structure to organized cognitive processes must be supported by data connecting α indices to task performance or task constraints. For example, one study looked at the relationship between pink-noise and task performance in a visual search task, and found that α was correlated with task performance on a trial-by-trial basis (Stephen & Anastas, 2011). These findings have been interpreted as suggesting that ocular fluctuations at relatively small time scales have implications for task performance at larger scales, and may support the efficiency of the cognitive system. The authors also suggest that if visual search performance is predicted by pink noise, then performance is as deeply rooted in lower-order oculomotor variability as it is in cognitive and neural structures.

The one study that examined 1/f scaling in children reported that children (mean age=24 months) showed higher α when watching blocks (α=1.28 +/- 17) than when watching faces (α=1.19 (+/- 17) (Wang et al., 2014). That same study found the opposite finding in adults, such that their α was higher when viewing faces than blocks. Importantly, they found similar variability in α for adults and children, suggesting that α is not a person-level stable trait, but instead is a property reflecting interactions between an individual and her environment.

There is also a small body of work that has measured the variance in the fractal structures of eye-gaze data to look for evidence of cross-scale interactions, either by measuring spectrum width or examining distributions of eye-gaze data. Adults' eye-gaze

data showed significant variance in α (e.g., a non-zero spectrum width) during a challenging visual search task where trials lasted up to five minutes (Amor, Reis, Campos, Herrmann, & Andrade, 2016). Spectrum width of eye-gaze data can also be manipulated by task constraints. One study that used data from saccade tasks found that the spectrum width of adults' eye-gaze data was reduced in the task that required decision making relative to the simpler saccade task, suggesting that increasing cognitive load can diminish cross-scale interactivity (Stan et al., 2014). Another study inferred system dynamics from the probability distribution functions (PDF) of eye-gaze data (as opposed to time series), using a method that places a system on a continuum from component-dominant (normal PDF) to interaction-dominant (power law PDF) (Stephen & Mirman, 2010). Between these ends of the continuum are lognormal PDFs which arise from interaction-dominant systems under task constraints. Overall, most participant's PDFs showed the best statistical fit with a lognormal distribution. However, in the task that was designed to be more challenging and place weaker constraints on the system (e.g., elicit more variable behavior), the PDFs were closer to a power-law distribution. These findings are consistent with the idea that when there are fewer task constraints, systems appear to be more interaction-dominant.

The present study

In the present study, there is variability in the external task constraints that the infants face, as well as internal developmental constraints that have the potential to

impact their attention system dynamics. In Study 1, I model how these factors impact measures of interactivity in time series of infants eye-gaze data.

My past work validated the use of Detrended Fractal Analyses (DFA) to examine scale-invariance in infants' eye-gaze (Stallworthy et al., 2020). In that study, we used longitudinal eye-tracking data from 166 infants (333 visits) from 3- to 36-months as they watched movies of women dancing, pixelated versions of those movies with diminished social content, and attention cues. We found that gaze patterns of even the youngest infants exhibited fractal organization, and that fractality increased with age. Fractal organization was also higher when infants viewed social stimuli, suggesting that in addition to the stable increases in α over developmental time, infants' gaze patterns are more self-organized when watching movies with richer social content. Importantly, there was also significant within-person changes in fractal organization, such that infants were more self-organized during times when they showed increased spontaneous attention to faces.

The present study seeks to replicate those findings with a larger sample by including visits collected since January 2018. Additionally, this study builds upon that work by meeting two aims. The **first aim** seeks to determine the minimum amount of data needed for DFA. My past work adhered to the standing recommendation for biomedical time series, and included time series with a minimum of 1,000 contiguous data points (Ihlen, 2012); however, it is an open question as to whether the same minimum data criteria should be applied to all kinds of data. Using sensitivity analyses

on real and simulated eye-tracking time series, I will determine the minimum number of

data points required for stable estimates of α.

The **second aim** seeks to examine developmental changes in cross-scale

interactivity, as measured by the multi-fractal (MF) spectrum width. Given that

hierarchical models of attention (Error! Not a valid bookmark self-reference.) emphasize

interactions between bottom-up and top-down attentional processes which are known to

occur on different time scales (Amso & Scerif, 2015), developmental changes in MF

width may be a better index of increased interactivity between these system components.

Using multi-fractal detrended fluctuation analysis (MFDFA) I will determine whether

these time series are multifractal, and if so, how MF spectrum width changes over time.

Methods

Research design

Participants. All participants were recruited from the Institute of Child Development's

participant registry at the University of Minnesota as a part of a larger mixed cross-

sectional and longitudinal study. Two primary cohorts were included. The first cohort

was part of a larger mixed cross-sectional and longitudinal study of brain and behavioral

development. The second cohort was part of a cross-sectional study on behavioral

development only. Participant exclusion criteria for Cohort 1 included: (1) history of

known genetic syndromes associated with ASD risk; (2) significant medical conditions

affecting growth, cognitive development, or significant vision or hearing impairment; (3)

birth weight < 2000 g and/or gestational age < 36 weeks; (4) history of significant

perinatal adversity, or exposure in-utero to neurotoxins; (5) having been adopted; and (6)

family history of a first-degree relative with intellectual disability, autism, psychosis,

schizophrenia, or bipolar disorder; (7) contraindication for magnetic resonance imaging.

Criteria for Cohort 2 were identical, with the exception of (7). Parents provided written

and informed consent for their child's participation in the study. All protocols are in

accordance with relevant guidelines and regulations and were approved by the University

of Minnesota's Institutional Review Board (IRB).

As part of a planned missingness design, children contributed between 1 and 6

waves of data during visits to the lab. More information on the samples used in Aims 1

and 2 can be found in those sections.

Procedures. At each visit, infants were seated in their parent's lap approximately 65 cm

from a 27-inch 1920×1080 resolution ASUS monitor that subtended 43.6 degrees of

visual angle with an aspect ratio of 16:9. Infants' eye movements were recorded with

non-invasive corneal-reflection binocular eye-tracking equipment (Tobii TX300,

recordings sampled at 300 Hz; Tobii Studio; Tobii Technology, Danderyd, Sweden).

They watched four 20-second movies of women dancing to lively music while waving

toys, as well as pixelated versions of these same videos. These two stimulus conditions

(Social and Pixelated; **Figure 3**) were used to compare the fractal structure of gaze

patterns while viewing social stimuli, relative to stimuli with most of the social

information degraded. Movies were interleaved with dynamic audio-visual attention cues

used for estimating recording accuracy and precision, and for establishing baseline levels

of infants' gaze organization. There were 4 different Social movies, each with a Pixelated

counterpart, for a total of 8 movies interspersed with audio-visual attention cues, as

shown in Figure 3. The entire eye-tracking task lasted approximately 5 minutes.
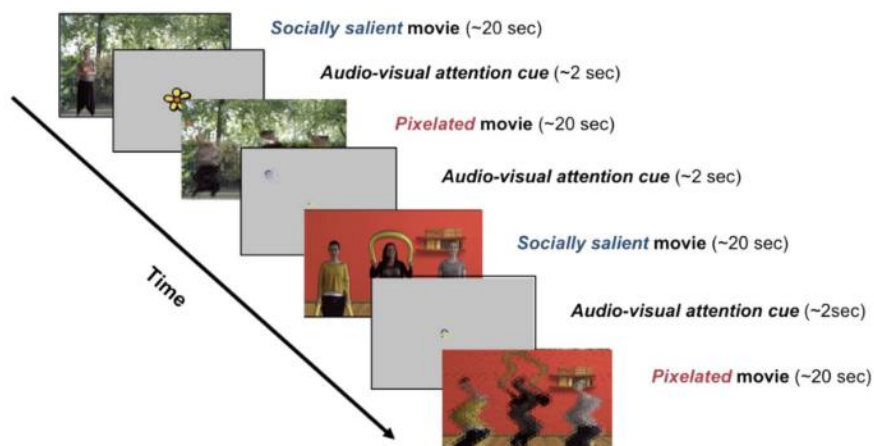
Figure 3. Example of the sequence of stimuli presented at each visit.
Socially salient movies featured women moving with toys. Pixelated versions of these movies were inter-
leaved with the socially salient movies. Movies were interleaved with dynamic audio-visual attention cues

Data Cleaning & Processing

Time-Series Generation. After the eye-tracking data were collected, we created gaze-

based time-series using the amplitude of change in infants' raw gaze position, sampled

every 3.33 ms, over time (as shown in **Figure 4**). As implemented, DFA does not allow

for missing data points. As in our previous work, to maximize the number of usable time-

series, eye-tracking data from each movie were divided into approximately 6-second

segments for analysis. Of the 4 movies, 3 were divided into 3 segments (mean=

7.38/SD=2.15 sec long), and 1 movie was divided into 4 segments (mean=6.47/SD=1.58

sec long) based on events in the movies. All Social movies and their Pixelated

counterparts were segmented for analysis, as was each audio-visual attention cue.

Blinks were identified using a noise-based algorithm (Hershman, Henik, & Cohen, 2018).

All data missing as a result of blinks (less than 200 ms) were linearly interpolated. The

longest contiguous stream of eye-tracking data for each movie segment was used to

generate the final time series used for DFA. As in our previous work, we used the

amplitude of change in gaze position over time as our time-series in order to account for

changes on both the X and Y axes, to avoid excessive computation and difficulties

interpreting our outcome for fractal organization along just one axis.
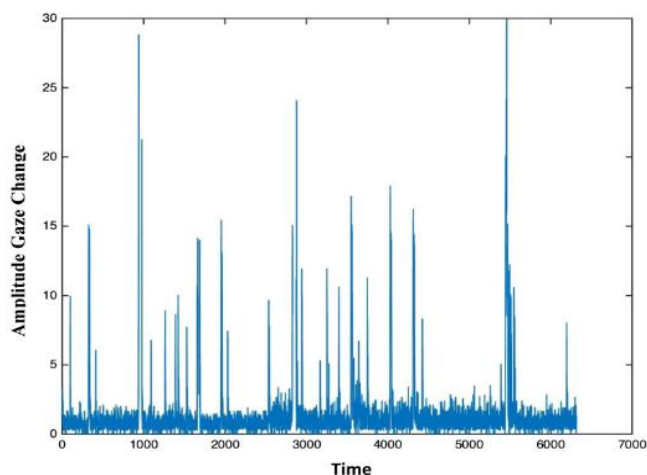
Figure 4. Example of a time-series comprised of the amplitude of X- and Y-coordinate gaze change. Amplitude is calculated as the change in Euclidian distance between two samples $D = sqrt((X_2 - X_1)^2 + (Y_2 - Y_1)^2$, relative to the change in time between samples, $T = t_2 - t1$ for the entire data stream, D/T) over time (1/300th of a second from a 300 Hz sampling rate).

Detrended Fluctuation Analysis (DFA)

DFA was performed on the time-series derived from each movie segment, using a

MATLAB package created specifically for biomedical time-series (Ihlen, 2012). This

analysis estimates the power law exponent that defines the scale-invariant, or fractal,

structure of a time-series. First, the time-series (amplitude of X and Y coordinate gaze

change over time) is converted to a random-walk-like structure by subtracting the mean

value and then taking the integral. Next, the time-series is divided into 4 equal-sized non-

overlapping windows, and a polynomial trend (m=2) is fit to each window of data. The

local root mean square (RMS) is then computed for the residual variation for each

window of data. This process is then repeated for increasingly smaller window sizes,

such that the relationship between amplitude of the residual noise and window size can be

ascertained.

DFA identifies the monofractal structure of the time-series as the power law

relation between the overall RMS's computed for multiple window sizes (**Figure 2**). This

power law relation is indexed by α or the slope of the regression line fit to the

log(frequency) and log(power) of the variation in the time-series. α denotes how fast the

local RMS changes with increasing window sizes, summarizing the long-term memory of

the series and quantifies the monofractal structure of a time-series on a continuum from

white noise (a ~0.5), through 'pink noise' (a ~0.8), to brown noise (a ~1.5) as shown in

Figure 5.
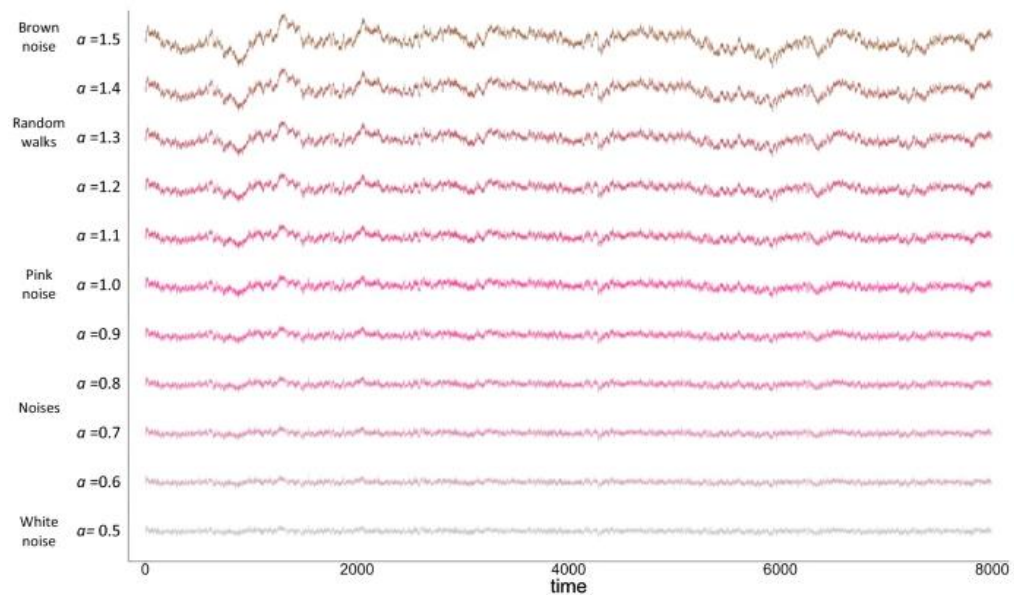
Figure 5. Visualization of time-series with different organizational structures from white noise, through pink noise, to brown noise with corresponding α values.

Multi-fractal Detrended Fluctuation Analysis (MFDFA)

To determine whether a time series exhibits change in the fractal scaling exponent over time, I used the direct determination method of the f(α) spectrum method (Chhabra & Jensen, 1989). This method estimates α in the same way described in the *Detrended Fluctuation Analysis* section, but does so at a range of fluctuation sizes (q). The array of α values calculated at varying q's is the multi-fractal spectrum width. If α varies as function of q then it is has a "wide" spectrum width and is multifractal; if it does not, then the time series is monofractal (**Figure 6**). Conceptually, this approach works because monofractal DFA assumes that these local fluctuations are normally distributed. However, when the state of a system changes (e.g. if the participant's attention shifts), these local fluctuations become heterogeneously distributed, reflecting a period of large

behavioral variability (Ihlen & Vereijken, 2010). Thus, if a time series has multi-scale

interactions and is characterized by these periods of non-gaussian distributions of local

fluctuations, then calculating α at different fluctuation sizes (q) should yield a range of

values.
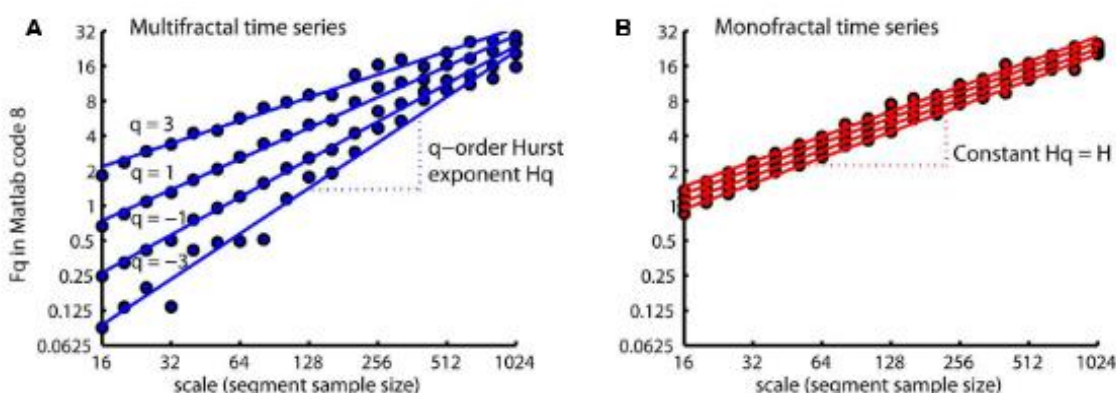
Figure 6. The scaling exponent α (described by the regression slope) calculated at different q's.
A shows a multifractal time series in which α varies as a function of q. **B** shows a monofractal time series
where α does not change as a function of q. Figure from Ihlen (2012).

Aim 1: Determine minimum amount of data needed for DFA

Methods

Participants.

For Aim 1, I used the same sample as the one previously published in Stallworthy et al.

(2020). Because the ultimate goal was to hopefully lower the threshold for the minimum

required time series length for DFA, I wanted to use infant eye-tracking data that had

passed the most stringent quality-related exclusionary criteria (**Figure 7**). For a more

detailed explanation of our quality-control exclusion criteria, please see the Aim 2

Methods section.

```
Original Sample
N= 190 (86 females)
Visits= 421
Time-series= 14,1870
```

```
Excluded for low eye-
tracker precision
N= 5
Visits= 28
Time-series= 939
```

```
Excluded for high
interpolation levels
N= 1
Visits= 1
Time-series= 2,788
```

```
Excluded for time-
series < 1000
N= 2
Visits= 8
Time=series= 2,223
```

```
Final Sample
N= 182 (84 female)
Visits= 384
Time-series= 8,920
```
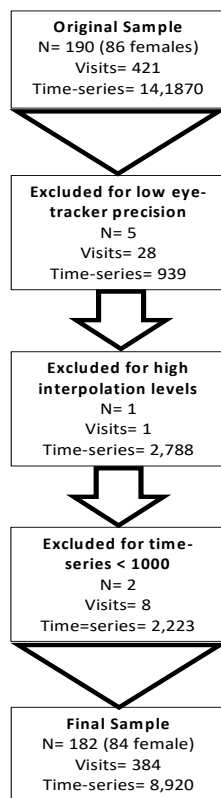
Figure 7. Flow diagram depicting the characteristics of the original sample from Stallworthy et al. (2020). Participants were sequentially excluded for low eye-tracker precision, high levels of interpolated data, and time series < 1,000 samples.

Selection of DFA parameters.

There are both statistical and phenomenological considerations when deciding on DFA input parameters. My past work selected these parameters based on general recommendations (Ihlen, 2012) and published empirical studies that used DFA to analyze eye-tracking data (Coey et al., 2012b; Wallot, O'Brien, Haussmann, Kloos, & Lyby, 2014). Prior to determining the optimal threshold for the minimum time series length, I visualized the impact of other parameters on estimates of α (**Table 1)** while holding the threshold for minimum time series length constant at 1,000 samples.

DFA calculates the size of changes in a time series at different scales (**Figure 8**),
and the parameters *scmin* and *scmax* determine the smallest and largest scales,
respectively. *Scres* then determines the number of scales at which *F* is calculated. To
examine how these parameters impact results, I calculated α using 32 different
combinations of parameters (*scmin*=4, 8, 12, 16; *scmax*= time series length/4, time series
length/10; *scres*=4, 8, 12, 16) for each time series. The range of each parameter was
selected to be inclusive of past recommendations. I then examined how each factor
impacted α and the goodness-of-fit of the linear scaling relationship (as indexed by the R^2
of the observed relationship between window size and RMS).

Parameter	Description	Parameter used in original manuscript	Values tested
*m**	Polynomial order for detrending at each window	2 (quadratic). Linear log2(scale)v log2(Fq)) plot indicated scale invariance compared to other m values.	N/A
scmin	Minimum window size for detrending	4 Based on previously published work by Wallot et al., 2015; Coey et al., 2012)	4, 8, 12, 16
scmax	Maximum window size for detrending	Length of time series/4 Based on Ihlen (2012)	Length/4, Length/10
scres	Total number of window sizes with which to detrend and calculate local RMS	4 Accommodates time-series closer to 1000 data points long.	4, 8, 12, 16

Table 1. Description of input parameters for DFA.
*The m parameter determines which polynomial order should be used for the detrending of the time series
prior to calculating RMS at each scale. In the original paper we used m=2 (quadratic detrending), because
the log-log plots of that this yielded scale invariance compared to the other m values. I opted to not
manipulate this parameter, since this was determined using visual inspection.
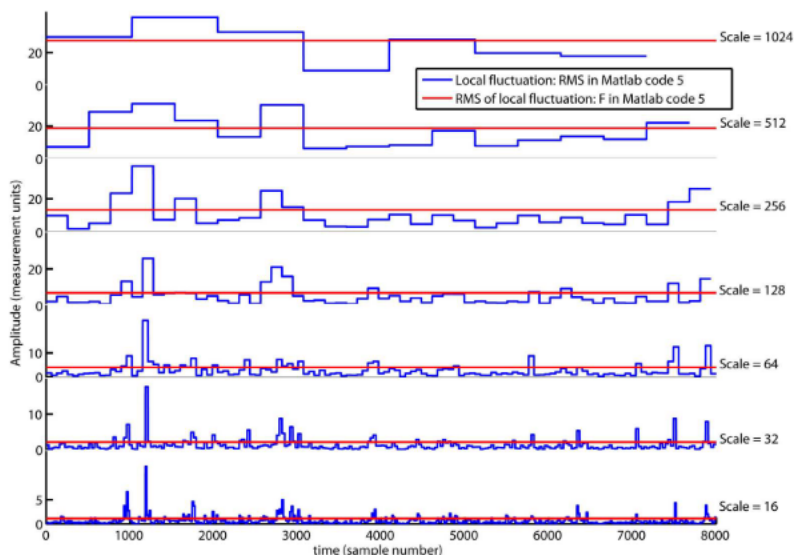
Figure 8. RMS is calculated at multiple scales defined by scres and scmax. for a time-series with 8,192 samples when scmin=16, scmax=1024, and scres=7.

At each scale: The time series is separated into n bins (n is determined by the scale, where n=time series length/scale). RMS is calculated at each bin. Then, the overall RMS is calculated for the time series (red line). At the smallest scale (16), the time series is broken up into 512 16-sample length bins (8,192/16). At the largest scale (1024), the time series is broken up into 8 1,024 sample-bins (8,192/1024). This is done 7 times (scale=32, scale=64 …).

Table 2 summarizes the mean and variance of α and R^2 estimates at each level of *scmin, scmax,* and *scres*. Mean α estimates were stable once the smallest segment size (*scmin*) was increased from 4 to 8; doing so decreased the average α estimates by 0.05, or 0.46 SDs. This corroborates past recommendations which note that when the minimum segment size is too small, α estimates get inflated (Ihlen, 2012). The *scmin* parameter had less of a meaningful impact on r^2 estimates, which ranged from 0.97-0.98 at all levels of *scmin,* indicating good linear fit. Moving forward, I adopted set *scmin*=8.

Changing *scmax* from length/4 to length/10 (thereby *decreasing* the maximum window size) led to slightly increased estimates of the mean and SD of α. To investigate this the impact of *scmax* for shorter and longer time series (defined by a median split of 1,654 frames) I plotted the relationship between *scmax* and α estimates as a function of

time series length (**Figure 9**). When the maximum segment size is too small α – as was the case for shorter fixations where *scmax* was set to length/10 rather than length/4) – estimates are more variable (and in rare cases have negative values). This parameter did not meaningfully impact R^2 estimates. Given these visualizations, I will continue using *scmax*=length/4.

Finally, increasing the total number of window sizes at which RMS is calculated (*scres*) did not have a meaningful impact on α or R^2 estimates. However, given that there is no reason to not increase this value other than increased computational burden, I doubled the number of window sizes from 4 to 8.

	Mean α	SD α	Mean r^2	SD r^2
scmin				
4	0.83	0.12	0.98	0.04
8	0.78	0.14	0.98	0.05
12	0.78	0.15	0.98	0.05
16	0.78	0.15	0.97	0.06
scmax				
Length/4	0.78	0.13	0.98	0.05
Length/10	0.80	0.16	0.98	0.05
scres				
4	0.80	0.14	0.98	0.04
8	0.79	0.14	0.98	0.05
12	0.79	0.14	0.98	0.05
16	0.79	0.14	0.97	0.05

Table 2. Impact of parameters (scmin, scmax, and scres) on α and r^2.
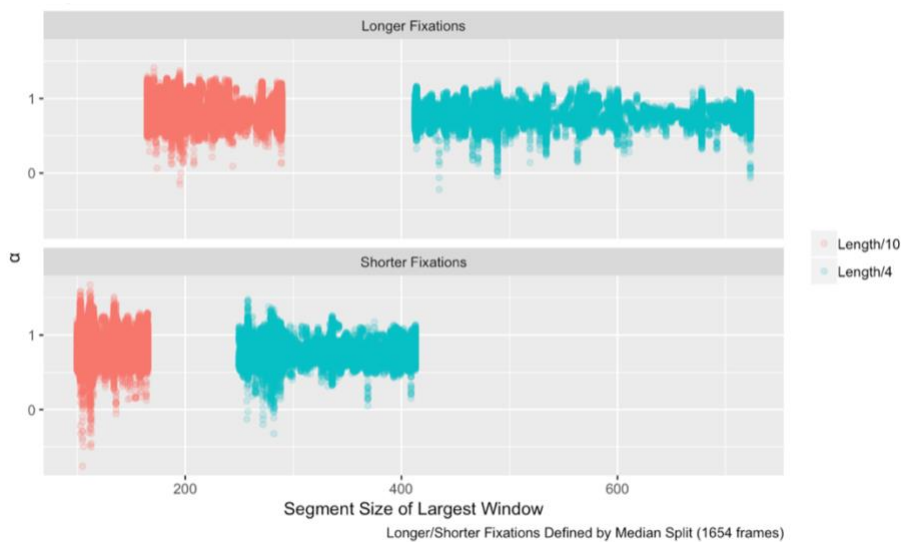
Figure 9. α plotted against the continuous length of the segment size of the largest window (*scmax*) for longest and shorter fixations.
For shorter fixations, setting *scmax* to length/10 (red) resulted in the largest window size being less than 200 samples, and less stable estimates of α.

Creating Truncated time series segments.

Each time series of length=*n* was truncated two ways (**Figure 10**). First, from the beginning of the time series ($X_{t=1}$) with truncated segments increasing by increments of 100 samples (e.g., {$X_{t=1}:X_{t=100}$, $X_{t=1}:X_{t=200}$, … $X_{t=1}:X_{t=n}$}). Then, time series were truncated from the end of the time series (e.g. {$X_{t=n-100}:X_{t=n}$, $X_{t=n-200}:X_{t=n}$, … $X_{t=100}:X_{t=n}$}). To ensure that each segment length increased by 100 samples, the original time series was truncated to ensure that *n* was divisible by 100 (e.g. the last 5 samples would be trimmed from a time series with 1,005 samples). This yielded (*n*/100)*2 – 1 truncated versions of each times series.

Truncated segments came from two types of time series: time series of real infant eye-track data and simulated pink noise. For the real eye-tracking data, the final sample from Stallworthy et al. (2020) was used. Each time series passed stringent quality control

assessments, and was at least 1,000 samples long. The final sample included data from

182 infants (84 female), 384 visits, and 8,920 time series (average length=1,685,

min=1,000, max=2,900) (**Figure 7**).

10,000 pink noise time series with a sampling rate of 300 Hz (the sampling rate of the

real eye-tracking data) were simulated using the tuneR package. The overall distribution

of time series length of the real eye-tracking data was modeled, so that the simulated time

series could be drawn from a similar distribution. Due to the skewed nature of the

observed distribution of real time series length, the parameters for a Johnson distribution

were estimated, and were then used to create a random distribution. The duration of each

simulated time series was determined by randomly selecting from the population

distribution of this random distribution.
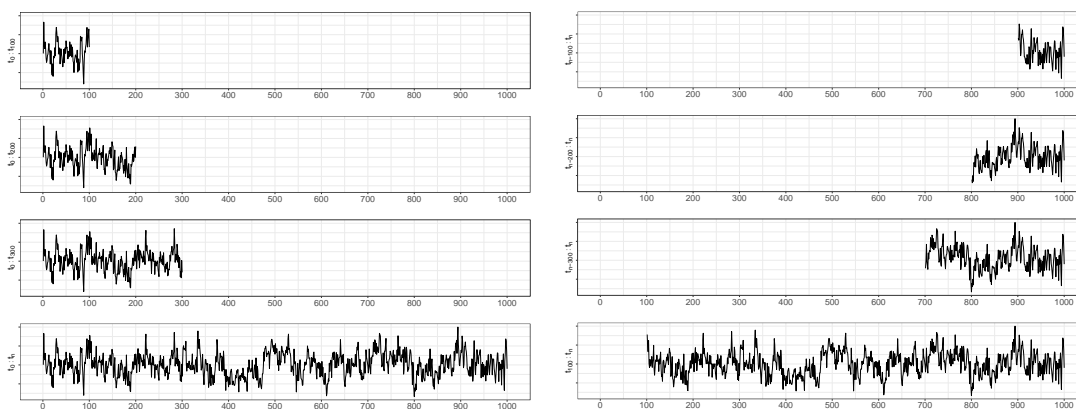
Figure 10. Schematic of how time series were truncated.

The bolded part of the time series indicates which section of the time series was used for to estimate α. Panels on the left depict removing the end of the time series, such that segments begin at t=1, and grow increasingly longer ($X_{t=1}:X_{t=100}$, $X_{t=1}:X_{t=200}$, … $X_{t=1}:X_{t=n}$). Panels on the right depict removing the beginning of the time series, such that segments end at t=n, and grow increasingly longer by starting earlier in the time series ($X_{t=n-100}:X_{t=n}$, $X_{t=n-200}:X_{t=n}$, … $X_{t=100}:X_{t=n}$).

Outcome Measures.

Our primary aim was to determine how the time series length (*n*) impacts the mean and variance of α estimates. Additionally, we examined the impact of *n* on the goodness-of-fit of the scaling function that determines α. This scaling function describes the relationship between segment size (frequency) and RMS (power). Importantly, DFA assumes that this scaling function is linear (**Figure 11**), and poorly selected input parameters can lead to a violation of this assumption (Ihlen et al., 2012). Thus, it is possible that including time series that are too short may also lead to a non-linear relationship between power and frequency. The R^2 of the observed relationship between segment size and RMS relative to the estimated linear function used to estimate α was used to index how well the observed estimates fit a linear slope.
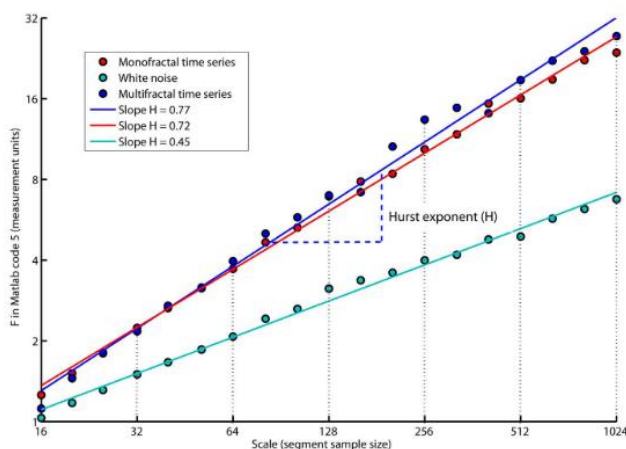
Figure 11. Figure from Ihlen et al. (2012).
The scaling function between sample size (X-axis) and overall RMS (Y-axis) is assumed to be linear. The data shown here fit a linear slope (e.g., the points measured at each segment size fit well with the linear slope).

Inclusion Criteria.

Both the number of truncated time series and the maximum length of truncated time series depends on the original time series length (n). Due to the minimum required data threshold (n≥1,000), each time series was able to be truncated into at least 19 segments (**Figure 12**). Time series longer than 1,000 samples generated more than 19 segments, and included truncated segments longer than 1,000 samples. For example, a time series with 1,200 samples would generate 23 segments ((1,200/100)*2-1) and longest truncated segment would be 1,100 samples long. To ensure that the effects of truncated time series length at longer lengths (e.g., 2,500 samples) were not just reflecting a minority of the sampled time series, truncated segments of a given length were retained if that length was able to be generated from at least 25% of the original time series.

Of the 8,920 real time series, 291,724 truncated segments were generated with an average length of 1,685 samples (min=1,000, max=2,800). Truncated segments with n≥2,200 were generated from fewer than 25% of the time series, and were excluded from analyses. The final sample included 278,441 truncated segments, with an average of 31 truncated segments generated for each time series (min=19, max=44).

The 10,000 simulated time series had roughly the same distribution of length as the observed sample of real time series (Average length=1,719, min=1,000, max=2,800). In the case of the simulated time series, truncated segments with n ≥ 2,300 did not reach the 25% threshold, however we excluded truncated segments with n ≥ 2,200 to be consistent with the analyses on the real eye-tracking data. The final sample of simulated data included 333,934 truncated segments, with an average of 33 truncated segments generated for each time series (min=19, max=55).
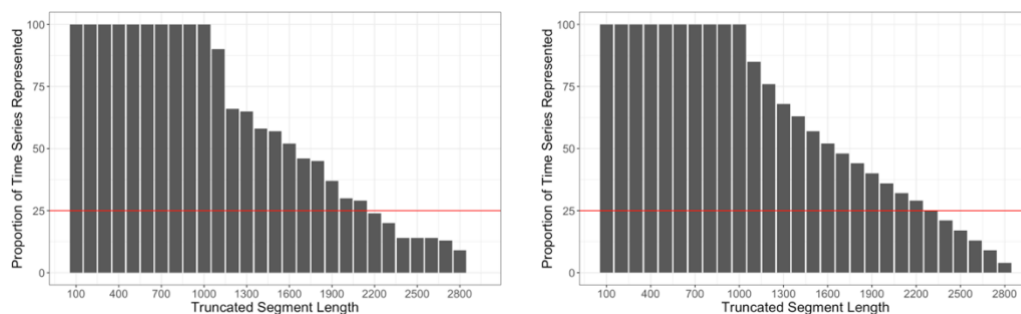
Figure 12. Proportion of truncated time series of each length.

All time series had a minimum length of 1,000 samples, and generated truncated segments of lengths {100, 200, … 1,000}. Truncated segment with length >1,000 therefore represented a proportion of the original time series sample. The figure on the left shows these proportions for the truncated segments generated from the real eye-tracking data, while the right shows these proportions generated from the simulated time series.

Analyses

α and R^2 were estimated for each truncated version of every time series, as described in *General Methods.* To determine the impact of time series length on average estimates of α, multi-level linear mixed effect models were estimated, with a random effect of intercept included for each unique time series (n=8,068). Separate models were estimated to determine whether a linear or quadratic effect of segment length (n), or an intercept-only model provided the best model fit. Model comparisons were conducted using chi square log likelihood ratio test and Second-Order Akaike Information Criteria (AIC; accounting for sample size and model complexity).

To determine the impact of time series length on the variability in estimates of α, a series of intercept-only multi-level linear mixed effects models were estimated with increasingly restricted datasets. First a model was fit using the whole dataset, then with all segments with n≥100, n≥200, etc. The intra-class correlations (ICC) was then calculated for each model. A high ICC indicates a greater proportion of variance in the

data is *between* time-series; in other words, there is more variability in α accounted for by the different time series relative to the variability observed across truncated segments within the same time series. On the other hand, a low ICC would indicate that a greater proportion of variance in the data is *within* time-series, which would suggest that including shorter segment lengths leads to more variable estimates of α.

Results

Impact of truncated segment length on R2

As expected, R^2 values (reflecting the correlation between the linear slope of α, and the observed relationship between power and frequency) were very skewed, and overwhelmingly indicated good model fit, with $R^2 \geq 0.9$ for 95% of the truncated segments generated from real data. With the exception of the 100-sample-long truncated segments, 56.9% of which had good model fit, all other truncated segment lengths had at least 91.8% time series with good model fit.

Unsurprisingly, 99% of the simulated pink noise time series data – which, by definition, should have a linear relationship between power and frequency – had good model fit. All of the truncated segment lengths with bad model fit were 100-samples-long, indicating that there is a lower limit for generating stable estimates of α even for simulated pink noise.

Impact of truncated time series length on mean estimates of α.

Analyses using real eye-tracking data indicated that the best fitting model included a quadratic term for segment length. For every 100-unit increase in segment length, there was a statistically significant but negligible increase in α ($B_{Length}=0.0023$, SE=7×10^{-5}), with the rate of change in α diminishing as segment length increased ($B_{Length^2}=-3\times10^{-5}$, SE=$3.7\times10^{-6}$, ΔLog-likelihood=177). To underscore how negligible this effect was, the estimated α at the maxima of the function (segment length=1,385) was 0.79, relative to 0.77 at the intercept (segment length=100).

Analyses using simulated pink noise time series yielded similar results. Again, the best fitting model indicated that there was a significant but negligible quadratic effect of segment length on α ($B_{Length}=0.0013$, SE=0.0004, $B_{Length^2}=-3\times10^{-5}$, SE=$3.7\times10^{-6}$, ΔLog-likelihood=325). Model results plotted over raw data can be found in Figure 13. Analyses were re-run excluding all truncated segment lengths with $R^2<0.9$, and yielded very similar results. Overall, with the exception of the very short truncated segment lengths, the truncated segment length had a minimal impact on average estimates of α.

a.

b.
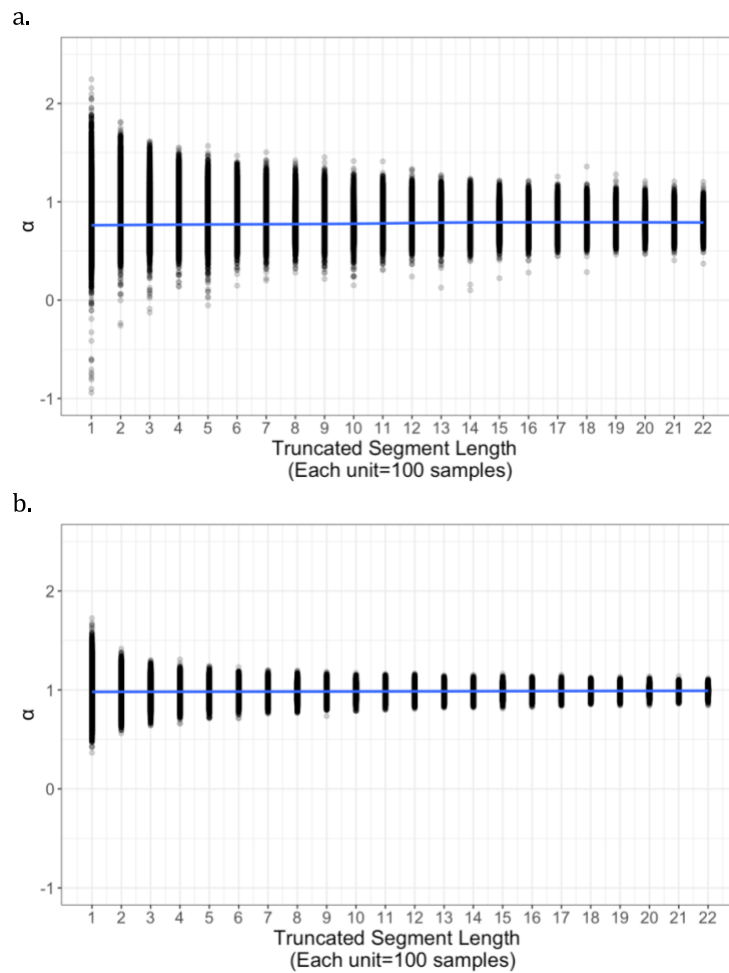
Figure 13.. Raw α distributions for each truncated segment length.
Distributions are plotted, overlaid with model results testing the relationship between truncated segment length and α for truncated segments generated from **a.** real eye-tracking data and **b.** simulated data.

Impact of time series segment length on variance in estimates of α. As can be seen in

Figure 13, while segment length has a minimal impact on the mean estimate of α, the

variance of α is quite high at shorter segment lengths.

Analyses using real eye-tracking data indicated that there was a quadratic effect of

increasing the minimum segment length when calculating the ICC of α. As the datasets

became more restrictive (e.g., ICC was calculated including segment lengths longer than 200, 300, 400, etc.), there was an increase in the proportion of variance accounted for by the time series ($B_{\text{Minimum Length}}$=0.179, SE=0.018, p=$2\times10^{-16}$), with this increase diminishing at higher thresholds ($B_{\text{Minimum Length\^{}2}}$=-0.0046, SE=0.0005, p=$2\times10^{-16}$) (Figure 14).

Because the coefficients in Beta regression are expressed as logits, to interpret these results the predicted ICC for each level of Minimum Length was back-transformed to probabilities (which in this case can be interpreted as the ICC, where $0 \leq \text{ICC} \leq 1$). When all time series were included in analyses, 50.7% of variance was *between* time series (e.g., the length of the truncated version was accounting for almost as much variance in α as the time series itself). For reference, when segments with length $\geq 1{,}000$ (the minimum required length suggested by Ihlen (2012)) were included, 79.7% of variance was between time series. The change in ICC from one minimum length to the next was plotted to determine if there were any "elbows" where the change in ICC begins to level off (Figure 14). Two potential elbows were identified – at Minimum Length=400 and 800.

Overall, similar findings were observed with the simulated time series. Again, as datasets became more restrictive, there was an increase in the proportion of variance accounted for by the time series ($B_{\text{Minimum Length}}$=0.071, SE=0.052, p=0.18), with this increase diminishing as the threshold was raised ($B_{\text{Minimum Length\^{}2}}$=-0.003, SE=0.001, p=0.004). In this case, elbows were identified ad Minimum Length=500 and 900.
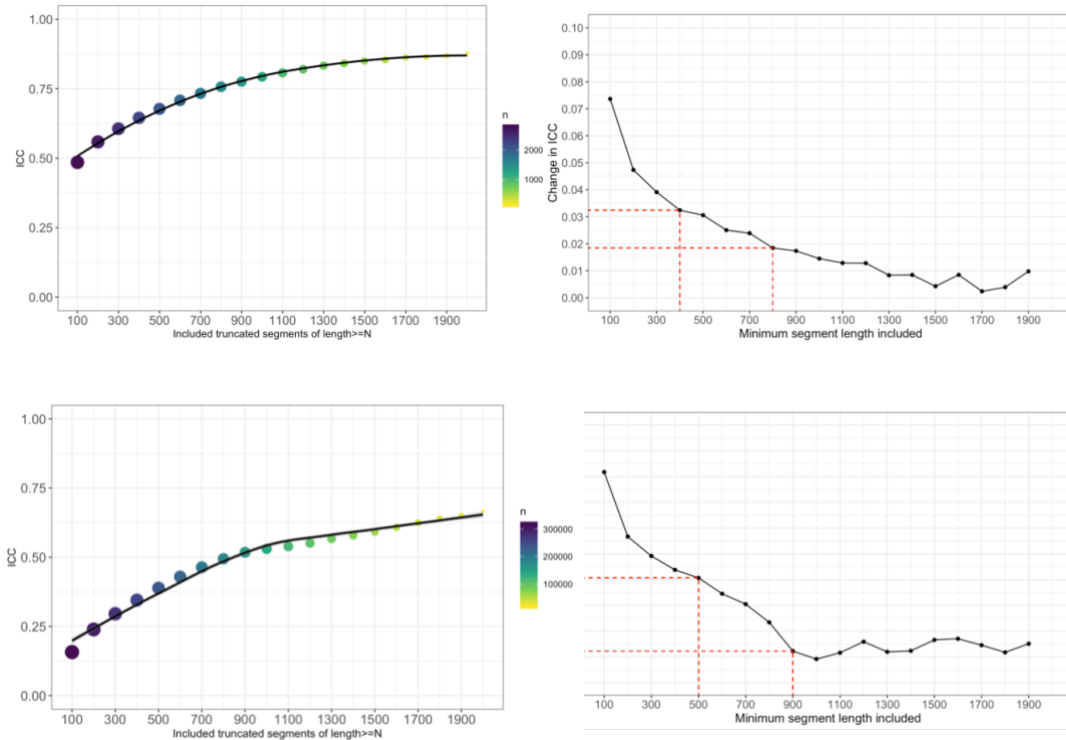
Figure 14. ICC estimates as a function of segment length.
Real eye-tacking data shown on the top row, simulated time series on the bottom row. **a.** The estimated ICC as a function of the minimum segment length thresholded are plotted over the observed ICCs. **b.** The change in ICC due to increasing the threshold of the minimum segment length is plotted, with identified elbows highlighted in the red dashed lines.

Aim 1 Conclusions

These findings indicate that the minimum time series length had a greater impact

on the stability of α estimates relative to mean α estimates or R^2. Minimum length

thresholds of 400 and 800 were identified as potential inflection points, where increasing

the minimum lengths led to more moderate increases in ICC thereafter.

When considering which minimum required length to adopt moving forward, a

few factors must be considered. Of the original sample of 14,187 time series, 2,223 were

excluded for having fewer than 1,000 frames. While decreasing the minimum required

length from 1,000 to 400 samples would have increased our sample by 1,116 time series (thereby recovering about 50% of the excluded time series), 400 samples of eye-gaze data collected at 300 Hz corresponds to only 1320 ms of data. Given that the aim of the present study is to understand visual exploration in infants, it is questionable whether including such short series has face validity.

Instead, for further analyses with this dataset, I will use a minimum required data threshold of 800, the second elbow in Error! Reference source not found.**a.** If we had included time series with length ≥ 800, this would have increased our sample by 439 time series, thereby recovering about 20% of the excluded time series). Though the elbow identified using the simulated time series is 900 segments, ICC increased minimally when the threshold was raised from 800 to 900. In an effort to retain as much data as possible, I will use the elbow identified in the analyses that used the real eye-tracking data.

Aim 2: Replicate DFA findings with a larger sample and wider age-range

Methods
Original Sample

This analysis included previously published data (Stallworthy et al., 2020), as well as data collected after the date of the last visit included in that manuscript (January 2018). The original sample included 32,151 time-series of eye-tracking data collected from 344 1.68-60.81-month-old infants (171 females, mean age= 16.23 months) across 903 visits to the lab. As part of a planned missingness design, children contributed

between 1 and 6 waves of data across this age span (mean 2.62 waves) during visits to the

lab (**Figure 15).**
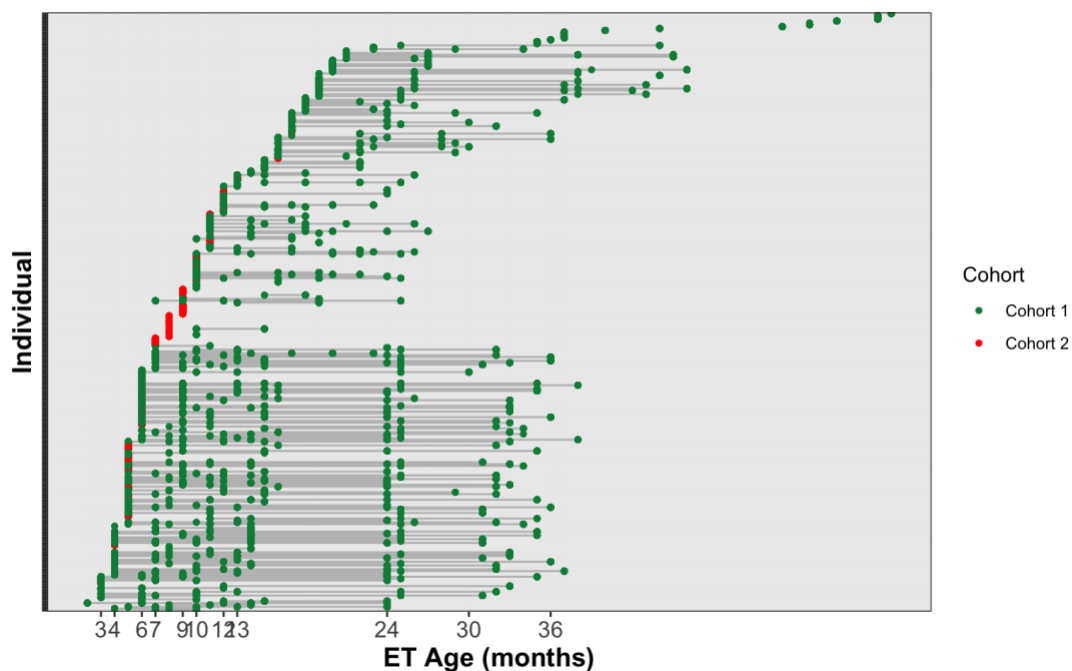
Figure 15. Final sample with eye-tracking data.
The majority of data came from Cohort 1, infants who were recruited for a brain imaging study (247 infants, 697 visits). Cohort 2 was comprised of infants recruited for a cross-sectional behavioral visit (72 infants).

Quality-control exclusion criteria. A detailed description of the quality-control

exclusion criteria can be found in Stallworthy et al. (2020). Broadly, time series were

excluded if an infant had poor eye-tracker calibration precision, if too much data were

linearly interpolated when generating the time series for DFA, if the time series were too

short (<800 frames, as determined in Aim 1), and if the time series' DFA yielded poor

linear fit thereby suggesting unstable estimates of α. Ultimately, I excluded 13,512 time

series for quality-control (42% of the original 32,151 time series). The final sample

included 18,639 time series (a 52% increase from the sample we have previously

published on). A flow diagram of the exclusionary process is shown in **Figure 16**.
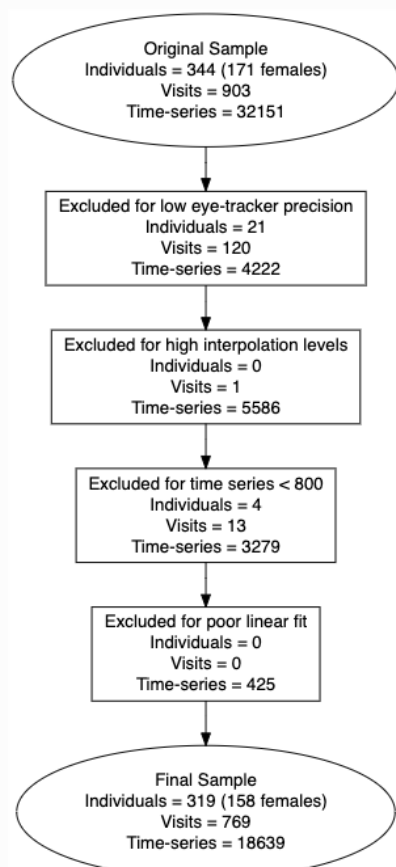
Figure 16. Flow diagram of the exclusionary process for Study 1, Aim 2.

Analytic plan.

As described in the general Methods section, α, or the linear relationship between

power and frequency, was calculated for each time series. I used linear mixed effects

models to examine growth in α across time. First, a model was fit with random effects for

all possible levels (person, visit, movie) to determine the proportion of variance

attributable to each level. Because only 2.9% of total variance was attributable to the movie grouping (relative to 11.6% to the person grouping, 23.0% to the visit grouping, with 62.5% accounted for by residual variance) I opted to only model random intercepts for the person (Level 3) and visit (Level 2), with variables related to the time series designated as Level 1 variables.

The exclusion criteria covariates that index eye-tracking quality were also tested at all appropriate levels. Level 1 control covariates included proportion of interpolated data, and the length of the longest contiguous sequence of gaze data used for DFA (both centered at the visit mean). Level 2 control covariates included the average proportion of interpolated data across a visit, the average length of the longest contiguous sequence across a visit, and the estimated eye-tracker precision (all centered at the person mean). Level 3 control covariates included the infant's average proportion of interpolated data across all of their visits, the infant's average length of the longest contiguous sequence of gaze data across all of their visits, and the infant's average eye-tracker precision across all of their visits (all centered at the grand mean),as well as their cohort and sex.

The goal of the first analysis was to examine age-related change in α, and whether growth curves differed as a function of stimulus condition (Social vs. Pixelated vs. Attention-cue). Therefore, the main predictors of interest were linear and quadratic effects of age, stimulus condition, and their interactions. I predicted that I would replicate the linear age-related increase in α from 3-36 months, and that with the increased sample size and age-range, we might see a quadratic effect of age where the increase levels out

after 36-months. Furthermore, with the 52% increase in time series contributing the analysis, we might be better powered to identify Age x Condition interaction effects.

Linear mixed effects models were fit in the following steps. First, I determined the appropriate functional form by for the fixed and random effects of age (linear and quadratic effects were tested). Second, I added in all potential control covariates into the model, and retained the covariates that were significantly associated with α. Third, I tested for effects of stimulus type (Pixelated, Attention Cue) with the Social stimuli as the reference group. Finally, I tested whether the growth rates differed as a function of stimulus type by testing for interactions between stimulus type and age. At each step, model comparisons were conducted using chi square log likelihood ratio tests and Second-Order AIC. Additional model parameters were retained only if AIC values and likelihood ratio tests indicated that adding them led to a model that better fit the data.

The goal of the secondary analysis was to test the association between α and spontaneous face-looking. To do this, we tallied the number of gaze coordinates recorded within the boundaries of the face areas of interest (AOIs) and the number of gaze coordinates recorded outside of these AOIs. These tallies were used to calculated the proportion of time spent within a face AOI relative to anywhere else on the screen. Open Source Computer Vision Library (Bradski, G., & Kaehler, 2008) was used to automatically identify face-related Areas-of-Interest (AOIs) for each movie-frame in the non-pixelated movies, and these same AOIs were applied to the movie's pixelated counterpart.

I then ran a second series of linear mixed-effects models, only including time series from the Social and Pixelated trials (n= 14,581 time series). Models were fit using the same steps as above, with the addition of four variables allowing us to examine the effects of face looking at all three levels: between-person face-looking (centered on the grand mean), within-person face-looking (centered on the individual's average face-looking), and within-visit face-looking (time series average, centered on the visit's average face-looking). I also tested for interactions between Face-looking and stimulus Condition.

Results

Fractal organization of the infant visual system

Scaling exponent α values were approximately normally distributed (skew = 0.34, kurtosis = 2.8), with a mean of 0.78 (range: 0.34–1.38). 73% of the time-series across all 3 conditions fell within what is thought to be the optimally flexible fractal, pink noise range (α ~ 0.7 to 1.0; Coey et al., 2012a; Ihlen, 2012). This proportion is notably smaller than the proportion found in Stallworthy et al. (2020), and is likely due to increasing the minimum window size (*scres*) from 4 to 8, as described in Aim 1.

Age-related change and effects of stimulus type on gaze complexity in stimulus

All model effects reported in this section are standardized coefficients (e.g. $B*(SD_y/SD_x)$). The baseline linear mixed effects model found α values increased with age ($B_{Age}= 0.29$), with growth in α decreasing over time ($B_{Age2}= -0.04$, $\Delta LL=81$, p=0.001). After adding a series of quality control covariates and retaining significant

effects (Table 3, Model 2), I assessed the effects of Stimulus condition on α. There were significant fixed effects of stimulus type, such that α was lower when infants watched Pixelated movies and Attention Cues relative to the Social movies ($B_{Pixelated}$=-0.11, $B_{Attention-Cue}$ = -0.13, ΔLL=266, *p*=2.2e-16).

A significant Condition x Age interaction (**Figure 17**) indicated that growth in the fractal organization of infants' eye gaze differed across stimulus type (ΔLL=25, *p*=2.5e-05). Tests of simple slopes suggested that while positive linear growth in α occurred for all Conditions (i.e., Social *b*=0.20, p=1.3×10^{-16}; Pixelated *b*=.12, p=9×10^{-5}, Attention-cue *b*=0.065, p=1.4×10^{-2}), the slope was significantly greater in the Social condition compared to both the Pixelated condition (Chisq=70.3, *p*=2.2×10^{-16}) and the Attention Cue condition (Chisq=92.15, *p*=2.2×10^{-16}). Additionally, simple slopes revealed the significant decrease in growth over time was limited to the Social condition (i.e. Social *b*=-0.06, *p*=0.01; Pixelated *b*=-0.01, *p*=0.68, Attention Cue *b*=0.02, *p*=0.50).

Predictors	Model 0 Estimate	SE	Model 1 Estimate	SE	Model 2 Estimate	SE	Model 3 Estimate	SE	Model 4 Estimate	SE
(Intercept)	-0.07	0.03	-0.01	0.03	0.01	0.02	0.01	0.02	0.01	0.02
Age			0.29	0.02	0.14	0.02	0.14	0.02	0.14	0.02
Age^2			-0.04	0.01	-0.01	0.01	-0.01	0.01	-0.01	0.01
Visit-level % interpolated					0.05	0.01	0.06	0.01	0.06	0.01
Visit-level fixation duration					0.04	0.01	0.03	0.01	0.03	0.01
Visit-level tracker precision					-0.18	0.01	-0.18	0.01	-0.18	0.01
Person-level fixation duration					0.04	0.01	0.03	0.01	0.03	0.01
Person-level tracker precision					-0.29	0.02	-0.29	0.02	-0.29	0.02
Condition=Pixelated							-0.11	0.01	-0.12	0.01
Condition=Attention-Cue							-0.13	0.01	-0.15	0.01
Age x Attention-Cue									-0.06	0.01
Age^2 x Attention-Cue									0.02	0.00
Age x Pixelated									-0.04	0.01
Age^2 x Pixelated									0.01	0.00
ICC	0.35		0.31		0.20		0.20		0.20	
N	319 Participant		319 Participant		319 Participant		319 Participant		319 Participant	
	769 Visit		769 Visit		769 Visit		769 Visit		769 Visit	
Observations	18639		18639		18639		18639		18639	
Marginal R^2 / Conditional R^2	0.000 / 0.352		0.064 / 0.351		0.173 / 0.339		0.192 / 0.357		0.195 / 0.359	
AIC	-31957.192		-32115.192		-32414.768		-32941.092		-32983.912	
log-Likelihood	15982.597		16063.598		16218.391		16483.556		16508.973	

Table 3. Table of model evidence displaying the effects of age and each of the stimulus conditions on α values.
The Social condition is set as the reference event. Estimates are standardized. Model 4 is the final, best-fitting model.
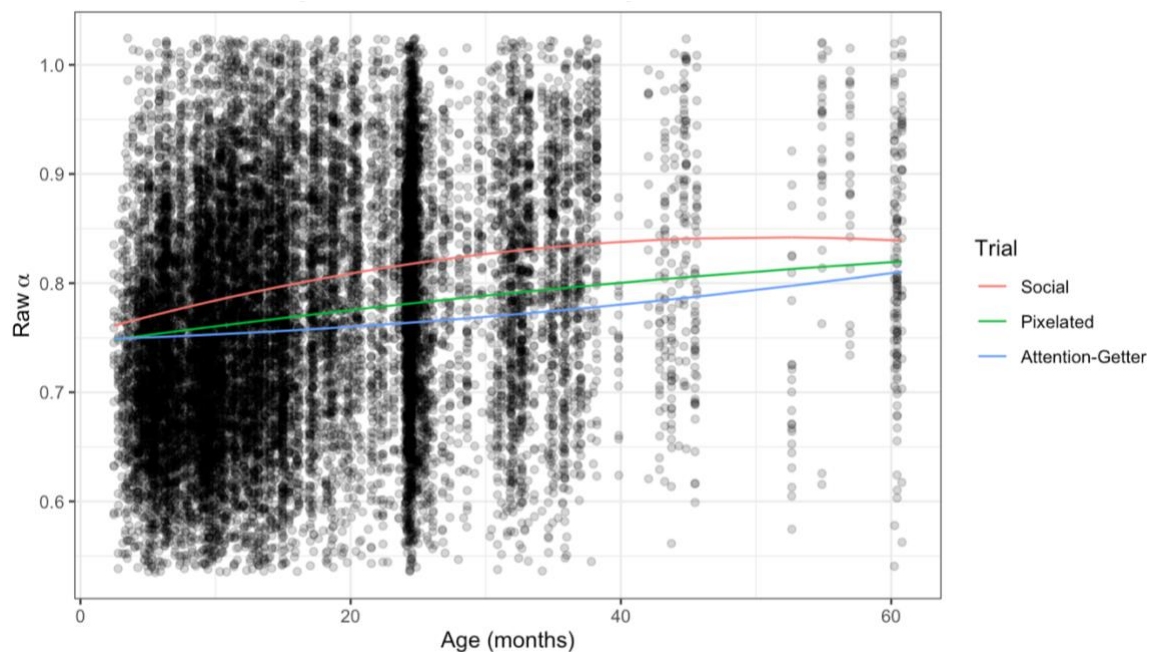
Figure 17. Effects of Condition x Age plotted over raw estimates of α.
Y-axis limits set to mean α +/- 2 SDs.

Visual complexity and gaze to faces.

Multi-level logistic regression was used to determine whether gaze location (on a face or

non-face region) varied between stimulus conditions. The baseline model found that the

probability of face-looking increased with age (ΔLL=179197, p=2.2e-16) by about 50.8%

each month. This model included a random effect of age, which accounted for 1.7% of

the between-person variance. As expected, infants spent less time fixating on faces during

the Pixelated condition (*b*=-1.66, a 16% reduced probability of looking at faces, all else

equal), compared to the same facial location during the social condition (ΔLL=873179,

p=2.2x10^{-16}). Finally, there was a significant Age x Condition interaction (*b*=0.004,

p=2x10^{-16}) indicating that while infants spent less time looking at the face AOI during the

Pixelated trials, age-related growth in face-looking was slightly greater for these trials.

In addition the growth trajectories of changes in α over time, I examined whether infants' spontaneous face-looking would correspond with changes in gaze complexity. To test this, I ran a second set of linear mixed effects models to examine whether there was a significant effect of time spent fixating on face relative to other areas of the screen on α (in addition to the aforementioned Age and Condition findings).

The best fitting model indicated that on average, α increased as a function of face-looking (ΔLL=25, p=4x10^{-11}) (see **Table 4** for full model results). This effect was significant at all levels (i.e. between-person, within-person, and within-visit face looking). The effect of face-looking on α also varied as a function of Condition (Δ LL=7, p=0.003). This interaction was significant for between-person face-looking (b=-0.02, p=0.009) and within-person face-looking (b=-0.02, p=0.01). These results indicated that infants who tended to spend more time attending to the face AOIs across all of their visits, on average, had higher α values particularly in the Social movies where the face AOIs contained richer social information (b Social=0.10, p=2x10^{-07}; b Pixelated=0.05, p=.006; Chisq=21.4, p=3.8x10^{-6}). Furthermore, during visits when infants spent more time attending to the face AOIs relative to their own average, infants had higher α values particularly in the Social movies (b Social=0.18, p=2x10^{-7}; b Pixelated=-.10, p=.006; Chisq=21.9, p=2.8x10^{-6}) (**Figure 18**).

Predictors	Model 0 Estimate	SE	Model 1 Estimate	SE	Model 2 Estimate	SE	Model 3 Estimate	SE	Model 4 Estimate	SE	Model 5 Estimate	SE
(Intercept)	-0.05	0.03	0.03	0.03	0.03	0.02	0.02	0.02	0.01	0.02	0.01	0.02
Age			0.33	0.03	0.17	0.02	0.17	0.02	0.14	0.02	0.14	0.02
Age^2			-0.06	0.01	-0.02	0.01	-0.02	0.01	-0.02	0.01	-0.02	0.01
Visit-level % interpolated					0.04	0.01	0.04	0.01	0.04	0.01	0.04	0.01
Visit-level tracker precision					-0.19	0.02	-0.19	0.02	-0.18	0.02	-0.18	0.02
Person-level tracker precision					-0.32	0.02	-0.31	0.02	-0.31	0.02	-0.31	0.02
Condition=Pixelated							-0.12	0.01	-0.11	0.01	-0.11	0.01
Within-visit Face-looking (%)									-0.02	0.01	-0.02	0.01
Within-person Face-looking (%)									0.07	0.02	0.07	0.02
Between-person Face-looking (%)									0.08	0.02	0.08	0.02
Within-visit Face-looking x Pixelated											0.01	0.01
Within-person Face-looking x Pixelated											-0.02	0.01
Between-person Face-looking x Pixelated											-0.02	0.01
ICC	0.39		0.34		0.22		0.25		0.24		0.24	
N	313 Participant		313 Participant		313 Participant		313 Participant		313 Participant		313 Participant	
	744 Visit		744 Visit		744 Visit		744 Visit		744 Visit		744 Visit	
Observations	14581		14581		14581		14581		14581		14581	
Marginal R^2 / Conditional R^2	0.000 / 0.390		0.079 / 0.390		0.202 / 0.378		0.210 / 0.406		0.223 / 0.407		0.225 / 0.408	
AIC	-26264.240		-26431.633		-26730.923		-27155.211		-27200.591		-27208.795	
log-Likelihood	13136.122		13221.819		13374.467		13589.616		13615.312		13622.421	

Table 4. Table of model evidence displaying the effects of face-looking and stimulus condition on α values. The Social condition is set as the reference event. Estimates are standardized. Model 5 is the final, best-fitting model.
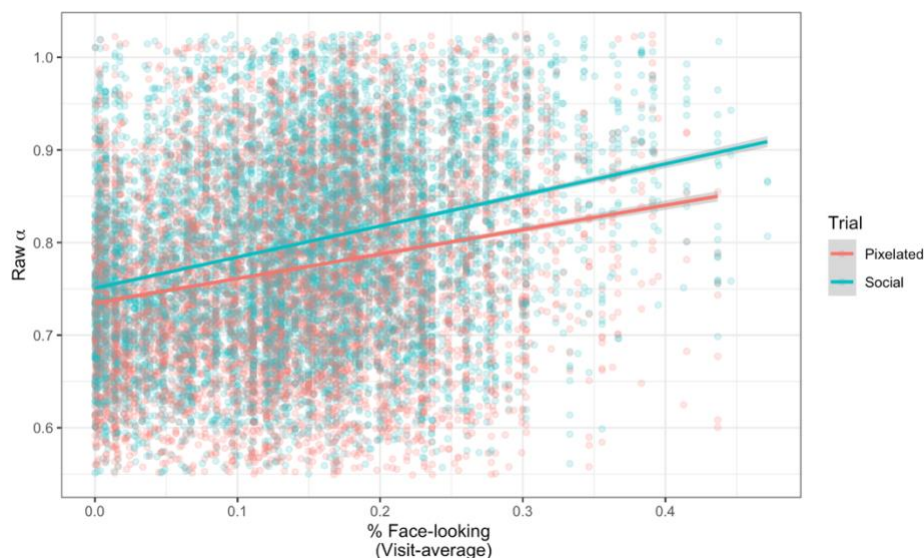
Figure 18. Estimated effects of within-person Face-looking x Condition plotted over raw estimates of α. Between-person face-looking variance is held constant. Y-axis limits set to mean α +/- 2 SDs.

Aim 2 Discussion

Overall, these results are similar to our past findings on age-related growth in eye-gaze

fractality. By increasing the sample age-range and including older children, I am now

able to model the decay of the age-related growth in fractality. This pattern corroborates

other's findings that infants' attention becomes more predictable and focal over the first

year of life when watching movies with social content (Frank, Vul, & Johnson, 2009), but

that predictability is more stable from 12-30 months (Frank, Vul, & Saxe, 2012). I also

found that the Social movies elicited increased fractality relative to both the Pixelated

movies and Attention cues, perhaps due to their more engaging content. The growth

curve for the Social condition also differed in two ways: First, the initial linear increase

was steeper, and second there was a significant decrease in growth rate over

developmental time. While the engaging social content may initially boost the self-

organizational properties of infants' eye-gaze, the self-organizational properties become more similar across the conditions as infants' attention abilities develop.

One noteworthy difference from Stallworthy et al. (2020) is that in the present sample the effect of face-looking on α was modulated by stimulus condition. While the proportion of time spent in the face AOIs was positively associated with α in both conditions, this effect was stronger for α values calculated from the Social movies. In other words, infants saw a greater increase in their eye-gaze fractality when attending to an area of the screen with rich social information relative to when they were looking at the same region but with degraded/pixelated social information. Given the small effect size of this interaction, it is possible that we were underpowered to detect it in our previous work.

Aim 3: Examine development of multi-spectrum width in infants

Methods

Calculating multi-fractal spectrum width

To estimate the multifractal (MF) spectrum width, a set of exponents are applied to the local fluctuations (RMS) ($q=\{x^{-5}, x^{-3}, x^{-1}, x^0, x^1, x^3, x^5\}$), and the scaling exponent (α) is calculated at each of these q-order statistical moments. Though there is debate over which range of q's should be used to estimate spectrum width (Ihlen & Vereijken, 2010), I used the range recommended in Ihlen (2012) for biomedical time series. The MF spectrum width was then calculated for each time series as the difference between the largest and smallest $H(q)$.

Comparison to linear surrogates

Because biological time series with 1/f power law scaling (e.g. pink noise) can sometimes

yield spurious non-zero multifractal spectrum widths (Ihlen & Vereijken, 2010), it is

important to statistically validate the observed multifractal spectrum width. To do so, I

generated eight surrogate time series for each original eye-tracking time series using the

iterative amplitude-adjusted Fourier-transform algorithm (IAAFT; Schreiber & Schmitz,

1996). This method reorders the original values in a way that preserves the average

power-law scaling and probability density function, while disrupting the original

temporal sequence.

As in previous work (Eddy & Kelty-Stephen, 2015; Ihlen & Vereijken, 2010), I

used these surrogates to test the null hypothesis that the original time series' MF width

did not statistically differ from the linear surrogate data's MF width. Using this

framework, if a time series yields a non-zero spectrum width *that does not fall within*

95% confidence intervals of the widths generated by its linear surrogates, then this would

indicate the presence of non-linear multi-scale interactions. I used a one-sample two-

sided t-test comparing the original data's spectrum width to the sample of linear

surrogates' spectrum widths was used, and coded t-statistics with *p*<0.01 as significant.

In addition to statistical significance, the size and sign of the t-statistic contains

information regarding the marginal difference between the original series spectrum and

the surrogate spectra (see **Figure 19** for an illustration). The size and sign of this

difference indicates how much the nonlinearity expands or contracts behavioral

variability within a task space. Simulation studies have shown that nonlinear interactions can lead to the original spectrum width being significantly narrower than the surrogates' when the interactions across time counteract each other and restrict variability (Lee & Kelty-Stephen, 2017). Thus, when width$_{ORIGINAL}$ < width$_{SURROGATES}$ (indicated by a positive t-statistic) this indicates the presence of nonlinear interactions that stabilize behaviors. On the other hand, when width$_{ORIGINAL}$ > width$_{SURROGATES}$ (indicated by a negative t-statistic) this indicates the presence of nonlinear interactions across scales that tend to increase variability in behaviors (Kelty-Stephen, 2018).

The top and bottom 1st percentile of t-statistics were identified as extreme outliers and removed (n=414 time series). Of the 18,650 time series included the analysis, 11,843 (63.5%) had a significant t-statistic (e.g. one can reject the null that the width of the time series is equivalent to the width of its surrogates). Of these significant t-statistics, 5,241 (44.3%) were negative, indicating that the time series' MF-width was significantly greater than the distribution of its surrogate widths. The remaining 55.7% were positive, indicating that the time series' MF width was significantly lower than the distribution of its surrogate widths).

T−stat is not significant
(monofractal)

MF width
original series

MF width of surrogates

T−stat is significant & positive
(multi−fractal stabilizing)

MF width
original series

MF width of surrogates

T−stat is significant & negative
(multi−fractal destabilizing)

MF width
original series

MF width of surrogates
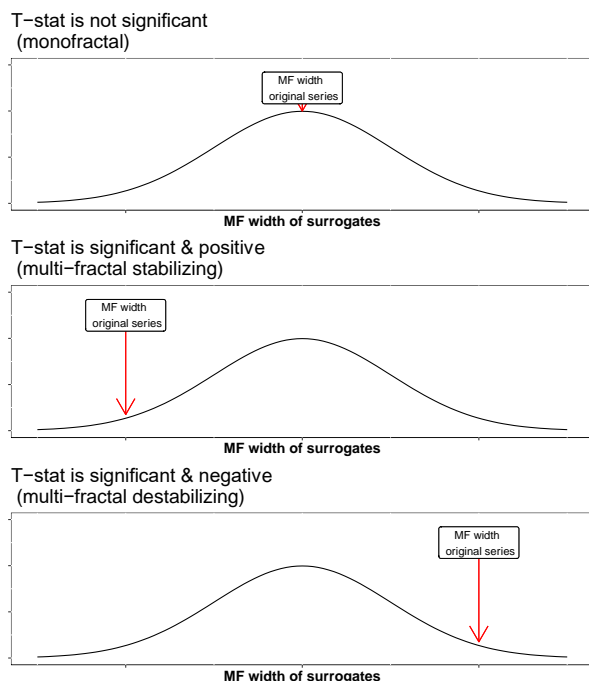
Figure 19. Example of spectrum widths and the t-statistics that they yield.
An MF spectrum width that falls within the distribution of its surrogates' spectrum widths would yield a non-significant t-statistic (e.g., the MF width is not significantly different then the surrogate distribution). An MF spectrum width with a value *lower* than 5th percentile of the distribution of spectrum widths yields a significant positive t-statistic (e.g. the width is significantly lower/narrower than the surrogate distribution). An MF spectrum width with a value *higher* than the 95th percentile of the distribution of spectrum widths yields a significant negative t-statistic (e.g. the width is significantly higher/wider than the surrogate distribution).

Analytic approach

Visualizations suggested that negative t-statistics (width$_{ORIGINAL}$ >

width$_{SURROGATES}$) were overrepresented in young infants (**Figure 20**). To model changes

in the class of time series (t$_{MF=}$non-significant/monofractal, significant

positive/multifractal stabilizing, significant negative/multifractal destabilizing) the

number of each class of time series was tallied for each visit. To test for effects of

stimulus Condition, tallies were calculated separately for each condition (Social,

Pixelated, Attention-cue). I then used a mixed-effects Poisson regression to estimate the

count of t-statistics in each class. The tallies of each class of t-statistic was entered at Level 1 variables, which were grouped within each infant (Level 2).

Next, I tested for interactions between t_{MF} and Age to determine whether the number of each type of time-series changes as a function of age. I then tested for interactions between t_{MF} and stimulus Condition (Pixelated, Attention-cue, with Social as the reference group) to determine whether the number of each type of time-series varied between conditions.
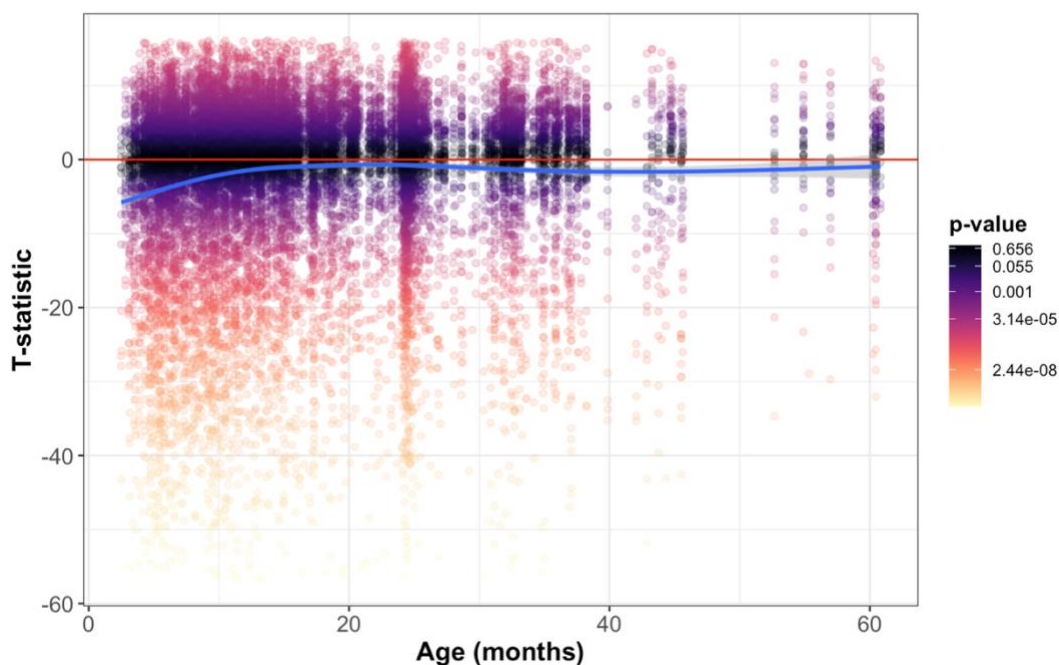
Figure 20. T-test statistic comparing the MF spectrum width of a time series against the distribution of its surrogates' (n=8) MF spectrum widths.
Significant negative values indicate that the time series' width is *greater* than the surrogate widths, indicating multi-scale interactions that tend to increase variability in system dynamics. Significant positive values indicate the time series' width is *narrower* than the surrogate widths, indicating multi-scale interactions that tend to constrain variablity in system dynamics. Non-significant values (shown in the cooler colors) indicate systems that do not have significant cross-scale interactions.

Results

Results for Poisson regression are reported in Table 5 with the significant positive t-statistics as the reference group (e.g., cases where width$_{ORIGINAL}$ < width$_{SURROGATES}$). As expected, the baseline model indicated that the relative odds of a time series having a significant negative t-statistic (e.g., width$_{ORIGINAL}$ > width$_{SURROGATES}$) compared to a significant positive t-statistic (e.g., width$_{ORIGINAL}$ < width$_{SURROGATES}$) was 0.78 (ΔLL=121, p=2.2x10^{-16}). The relative odds of a time series having a non-significant t-statistic (e.g. width$_{ORIGINAL}$ ≈ width$_{SURROGATES}$) compared to significant positive was 1.15 (ΔLL=42, *p*=2.2x10^{-16}). Put simply, these results confirm what was evident from raw counts; the number of time series where t$_{MF}$=Non-significant > t$_{MF}$=Positive > t$_{MF}$=Negative. As expected, these odds ratios diminished as infants got older (*b* Age x t$_{MF=n.s.}$=-0.004, *b* Age x t$_{MF=Negative}$=-0.012, ΔLL=37, p=6.6x10^{-16}). In other words, infants were less likely to have negative t-statistics (reflecting nonlinearity that *expands* variability) as they got older (Figure 21).

Next, I tested for interactions between t-statistic and stimulus Condition by adding main effects of Condition (Pixelated and Attention-cue, with Social as the reference group) and testing for interactions between t$_{MF}$=negative x Condition, then t$_{MF}$=non-significant x Condition, and then t$_{MF}$ =negative x Condition + then t$_{MF}$ =non-significant x Condition. The model including interaction terms for both t$_{MF}$ =negative and t$_{MF}$ =non-significant failed to converge, and was not included as a candidate model. Of the remaining models, the best-fitting model included the interaction for Condition x t$_{MF}$=negative (*b* t$_{MF}$=negative x Pixelated = 0.27, *b* t$_{MF}$=negative x Attention Cue = 0.20; ΔLL=668, p=2.2x10^{-16}). In other words, the finding that there were fewer negative t-

statistics (reflecting nonlinearity that *expands* variability) compared to positive t-statistics

(reflecting nonlinearity that *contracts* variability) was amplified in the Social condition

(Figure 22).

Predictors	Model 0 Incidence Rate Ratios	std. Error	Model 1 Incidence Rate Ratios	std. Error	Model 2 Incidence Rate Ratios	std. Error	Model 3 Incidence Rate Ratios	std. Error
(Intercept)	2.60	0.06	2.77	0.06	2.76	0.06	3.60	0.09
t-stat = n.s.			1.03	0.02	1.03	0.02	1.03	0.02
t-stat = negative			0.79	0.01	0.79	0.01	0.68	0.02
Age					1.01	0.00	1.01	0.00
Condition = Pixelated					0.99	0.00	0.99	0.00
Condition = Attention-cue					1.00	0.00	1.00	0.00
t-stat=negative x Age							0.83	0.02
t-stat=n.s.x Age							0.50	0.01
t-stat=negative x Condition=Pixelated							1.31	0.05
t-stat=negative x Condition=Attention-cue							1.22	0.05
ICC	0.25		0.25		0.26		0.24	
N	318 Participant		318 Participant		318 Participant		318 Participant	
Observations	6576		6576		6576		6576	
Marginal R^2 / Conditional R^2	0.000 / 0.255		0.031 / 0.278		0.040 / 0.285		0.189 / 0.380	
AIC	29865.352		29625.556		29557.794		28229.487	
log-Likelihood	-14930.675		-14808.775		-14771.888		-14103.723	

Table 5. Table of model evidence displaying the effects of age and each of the stimulus conditions on multifractality.
Models or linear mixed-effects Poisson models Estimates are converted to incidence rate ratios. Model 3 is the final, best-fitting model.
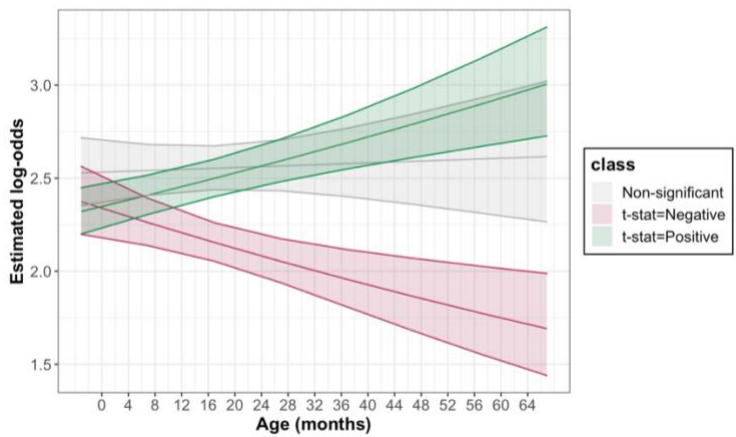
Figure 21. Interaction between Age and t-statistic type.
Trajectories show marginal means estimated from Model 3, with 95% CI. As infants got older, positive t-statistics were more likely and negative t-statistic were less likely.
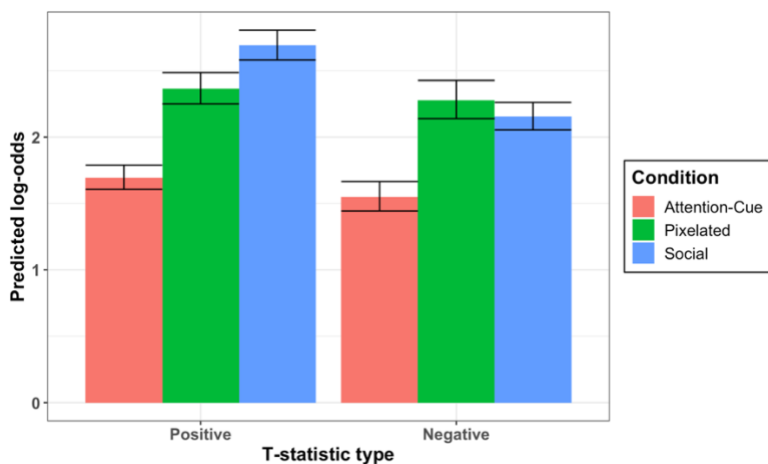
Figure 22. Interaction between Stimulus Condition and t-statistic type.
Bar plots show marginal means estimated from Model 3, error bars are 95% CIs. The decrease in odds of a negative t-statistic was greatest in the Social condition.

Aim 3 Discussion

Contrary to my prediction that infants' eye-gaze would show increased cross-scale interactions as they got older, there were age-related changes in the quality rather than the quantity of cross-scale interactions. Specifically, as infants got older their eye-gaze was more likely to show evidence of nonlinear interactivity that constrains system variability and less likely to show evidence of nonlinear interactivity that expands system

variability. These findings corroborate past work that has shown that entropy, or unpredictability, of eye-movements decreases as infants get older (Frank et al., 2009). At all ages, infants were more likely to show evidence of nonlinear interactivity that contracts system variability, particularly in the Social condition.

These findings support theoretical models of early visual social engagement. These theories posit that early attentional biases for social stimuli may reflect more "reflexive" sub-cortical attention pathways and *experience-expectant* development, whereas later-emerging preferences for social stimuli reflect more volitional and cortically-driven pathways shaped by *experience-dependent* development. Indeed, human newborns reflexively orient to social stimuli from birth (Bardi, Regolin, & Simion, 2011; Farroni et al., 2002; Valenza et al., 1996), suggesting that these early biases could provide infants with the early visual experiences with the social world that then tune cortical processing of social information. This bidirectional feedback loop occurs between bottom-up and top-down attention processes across timescales, and would theoretically yield more predictable orienting to social information. The present finding that infants are more likely to show cross-scale interactivity that constrains variability as they get older, and particularly when watching movies with social content, may reflect both an increase in interactivity between bottom-up and top-down attention, as well as increased experience with the social world.

Another potential explanation of these changes in cross-scale interactivity is changes in the frequency of saccades relative to fixations. Past work has shown that most of the non-linear interactivity in adults' eye-gaze data comes from saccades rather than

fixations (Amor et al., 2016). While this work differs from the present in that it did not use linear surrogates or distinguish between the quality of the cross-scale interactivity, it raises the possibility that some of these findings are related to age-related changes in more macro measures of eye-gaze. Future analyses will focus on better understanding the relationship between micro and macro gaze dynamics.

Discussion

There were four main findings from Study 1. First, from a methods perspective, I found that amplitude time series from 300 Hz infant eye-tracking data as short as 800 samples can reliably be used to estimate α for DFA (**Error! Reference source not found.**). Given the challenges associated with collecting data from infants, this finding has important practical implications for increasing the statistical power to detect both within- and between-person effects. Second, I replicated my past work showing that α increases linearly in the first three years of life (**Figure 17**). I then expanded on this work by including a wider age-range and a larger sample which allowed me to illustrate faster growth rates in the Social condition compared to both the Pixelated and Attention-cue conditions, and to model how this growth slows as infants get older. These results suggest that social content may elicit more fractally organized gaze strategies, particularly early in infancy when privileging social information may be particularly important for development.

Third, I replicated my past work showing that α increases with face-looking (**Figure 18**). This finding was true both between-infants (e.g. infants who looked at faces

more than the group average had increased fractal organization) and within-infants (e.g. infants who showed increased face-looking during a visit relative to their own average showed increased fractal organization). Importantly, with the larger sample I was able to model how this relationship was moderated by stimulus content, and was stronger when infants were watching movies with Social content. In other words, spending more time attending to the same area of the screen had a stronger effect on α when that area contained richer social content.

Fourth, I moved beyond DFA and modeled the multi-fractal spectrum width to determine whether infants' eye-gaze shows cross-scale interactions. Results from these analyses indicated that 63.5% of time series showed evidence of cross-scale interactivity, and that the kind of cross-scale interactivity changed as function of age and stimulus content (**Figure 21** and **Figure 22**). As infants got older they were more likely to show cross-scale interactivity that constrains system variability, and this kind of interactivity was more likely to be elicited in the movies with social content.

These findings should be interpreted in light of several limitations. First, the decay in growth rate reported in Aim 2 should be replicated with a sample that includes more data in infants older than 36 months. Second, given the challenges associated with distinguishing fixations from saccades -- both practically (Hessels & Hooge, 2019; Hessels, Niehorster, Nyström, Andersson, & Hooge, 2018) and conceptually (Kelty-Stephen & Mirman, 2013) -- the present study did not attempt to measure associations between these more macro measures of oculomotor movements and the fractal properties of eye gaze. This leaves open the possibility that changes in the relative proportions of

these eye movements may be explaining some of the observed effects. That said, the finding that the effect of face-looking on α is moderated by stimulus condition suggests that these effects cannot be wholly explained by oculomotor movements, since looking in the same AOI yields different results when that region of the screen has social information.

In summary, these results suggest that the visual attention system is well-organized in infancy. They also shed light on both endogenous factors (e.g. age, proclivity to look at faces) and exogenous factors (e.g., stimulus content) that can influence these properties. While these results focus on a typically developing population, future work with the Infant Brain Imaging Study (IBIS) network will examine whether these metrics can be used to predict which infants are more likely to receive a diagnosis for autism spectrum disorders (ASD). Additionally, I will investigate how the development of functional brain networks supports these attentional processes, as described in Study 2.

Study 2

Background

The development of visual selective attention is critical for effectively engaging with an ever-changing world, and is dependent upon interactions between systems across multiple timescales and loci. During the first years of life, infants make rapid strides in their ability to engage in visual selective attention: At birth, infants are only able to orient to external stimuli in their environment, but by the end of the first year of life they are able to flexibly deploy interacting attention mechanisms, balancing internal goals and external stimulus demands (**Figure 1**). These developments in attention have been well-documented using tasks designed to tease apart stimulus-driven and goal-driven attention (for a review, see Amso & Scerif, 2015), and using techniques designed to holistically measures system-wide complexity (Stallworthy et al., 2020).

These well-known changes in the dynamics underlying infants' attention systems coincide with rapid changes in functional brain connectivity. Resting state MRI (rsMRI) measures this temporal correlation in the BOLD signal between brain regions (Gao et al., 2017). The past decade has seen an explosion in research examining rsMRI in the developing brain (Zhang, Shen, & Lin, 2019). Most studies on changes in functional connectivity (FC) in the first years of life present cross-sectional evidence or 2-3 time points (Gao et al., 2011, 2009; Lin et al., 2008), with the exception of one longitudinal study examining growth in functional networks in 65 infants at 2 weeks, and 3, 6, 9, and 12 months (Gao et al., 2014). Together these studies have shown that FC increases

rapidly in the first years of life, with higher-level networks that may support more

experience-dependent processes (e.g. the lateral visual/parietal (V3), default mode (DM),

salience (SA), and frontal parietal (FP)) showing protracted development relative to

lower-level networks (e.g. sensorimotor (SM), auditory (AM), medial occipital (V1), and

occipital pole (V2) networks).

To my knowledge, no study has examined relationship between rsMRI and direct

measures of visual attention in infants. In Study 1, I presented results that changes in eye-

gaze fractality dynamically change with infants' spontaneous viewing patterns across

seconds, but that there were also slower changes across the first years of life that tracked

with between-person measures of age and face-looking. This raises questions about the

neural mechanisms that explain these between-person developmental changes in eye-gaze

fractality. The present study will examine the relationship between intrinsic functional

connectivity within and between specific networks in the brain, and their association with

fractal eye-gaze dynamics in infants.

Based on data from adults and children, as well as theoretical models of attention and

brain development in infants, I will focus on the default mode network (DMN), dorsal

attention network (DAN), salience/cingulo-opercular network (Sal/CO) and the fronto-

parietal control network (FPC).

The default mode network and the dorsal attention network

The DMN has been linked to Attention-Deficit/Hyperactivity Disorder (ADHD)

in adults (Castellanos et al., 2008) and elementary school aged children (Fair et al.,

2010), and the DAN has been linked to anticipatory attention (Maurizio Corbetta, Patel, & Shulman, 2008). Connectivity *within* both of these networks increases rapidly in the first year of life (Fair et al., 2008; Gao, Alcauter, Smith, Gilmore, & Lin, 2015), and connectivity *between* these networks has been shown to decrease in the first year of life (Gao, Alcauter, Smith, et al., 2015), and become more strongly negatively correlated (Gao et al., 2012). In adults, individual differences in the strength of the negative correlation between these networks in both resting and task conditions is associated with less variable performance on a flanker test (Clare Kelly, Uddin, Biswal, Castellanos, & Milham, 2008).

In Study 1 I presented evidence that the fractality of infants' eye-gaze increased over developmental time, and that infants are more likely to have spectrum widths that indicate nonlinear system dynamics that constrain behavioral variability as they get older. Given the developmental progression of increased negative synchrony between the DMN and DAN networks, I predict that stronger negative DMN-DAN connectivity will be associated with more positive t-statistics, or increased multi-fractal spectrum widths that indicate a contracting of behavioral variability.

The salience/cingulo-opercular network and frontoparietal control network

While the dorsal frontoparietal network has been implicated in goal-driven attention, the ventral frontoparietal network responds when an individual detects task-relevant visual information (Corbetta, Kincade, Ollinger, McAvoy, & Shulman, 2000). It has been argued that while both the dorsal and ventral streams are important for

catalyzing the development of the PFC (as they are both critical streams of visual

information), the ventral stream may explain more intra-individual differences given its

role in processing stimuli that are learned through social interactions (e.g. faces), and

labeled by caregivers (e.g. shapes, colors) (Rosen, Amso, & McLaughlin, 2019). I predict

that fractality and MF spectrum width in the Social Condition – but not the Pixelated

condition – will be associated with FC measures in these networks.

The present study

The present study will examine the relationship between intrinsic functional

connectivity within and between specific networks in the brain, and their association with

the increasingly self-organized eye-gaze dynamics observed in infants. Using densely

sampled longitudinal data collected from the Baby Connectome Project (Howell et al.,

2019), the present study will leverage fc-MRI and eye-tracking data to meet **two aims**: 1)

to model longitudinal growth in within-network functional connectivity, and 2) to

examine how changes in the self-organization of infants' eye gaze are supported by the

development of specific functional brain networks.

Methods

Participant recruitment.

All scans were collected from infants as part of the Baby Connectome Project (BCP), a

Lifespan Connectome Project funded by the NIH. The primary objective of the BCP is to

characterize brain and behavior development in the first 5 years of life. Children between

0-60 months were eligible for enrollment if they 1) were born between 37-42 weeks of gestational age, 2) did not weigh less than 2,000g at birth 3) had no major pregnancy or delivery complications, and 4) had no contraindication for MRI.

Data processing for the BCP data is on-going. As of March 2021, there were 349 processed scans with resting state data from 169 individuals (mean age=18.26 months, age-range=8-60 months). Data from infants younger than 9 months (n=18 scans) were excluded as the grey and white matter segmentation must be done by hand for this age group, and segmentation is on-going. 21 scans were excluded for having fewer than 600 frames, and 39 were excluded for not passing quality control. Finally, 54 scans were removed from the present analyses because they had to be re-processed due to an error. The final sample of available resting state data was 217 scans from 131 individuals (Figure 23).

Given that a significant number of scans will be added to this sample within the next few months, and that these scans will bolster the number of infants with at least three usable time points (one of the primary goals of the BCP), we expect the results to change substantially once we add these scans to the sample. Code is already written for these analyses (github.com/rrobinn/RS-Functional-Connectivity-Models/), so that analyses can be done immediately once the data are ready (this repo is private, please

email me for access). For the present dissertation, I will present the predictions and

analytic plan.
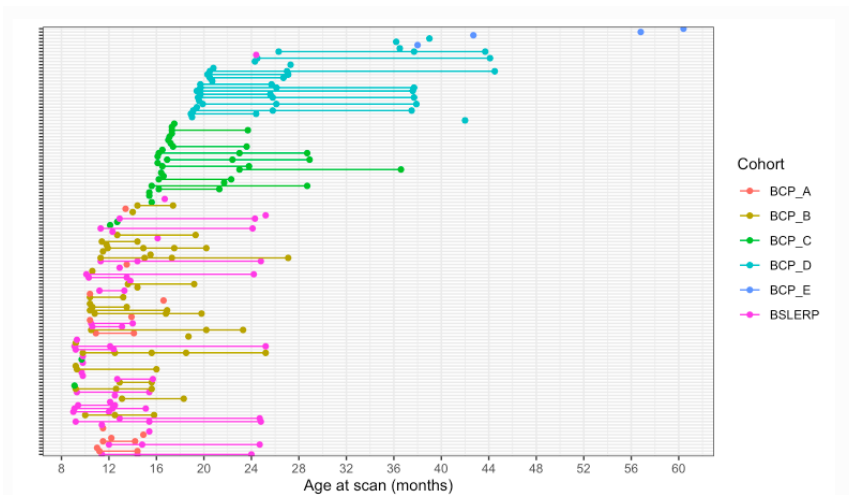
Figure 23. Sample of available scans with resting state data.
Each individual is colored by the cohort they belong to. BCP was designed as an accelerated longitudinal study where each cohort covers overlapping age ranges.

Imaging

Images were acquired on 3T Siemens Prisma MRI scanners using a Siemens 32 channel

head coil at the University of Minnesota Center for Magnetic Resonance Research. The

imaging protocol closely followed that of the Human Connectome Project (Van Essen,

Smith, Barch, Behrens, Yacoub, & Ugurbil, 2013).

For field maps and rsfMRI, data were collected in posterior-anterior (PA) and

anterior-posterior (AP) direction pairs. Data were acquired in the following order: T1-

weighted (MPRAGE), T2-weighted (T2wSPC), spin-echo field maps, rsfMRI, DTI, then

field maps and rsfMRI repeated identically and a second set of DTI scans. If data were

not of high enough quality (rsfMRI motion monitored with FIRMM; Dosenbach, et al.,

2017), reacquisition was attempted. If the child was unable to continue sleeping, the

second set was not always collected. Consequently, 114 scans had only one pair of

rsfMRI data (11:34 minutes of data); while 103 had at least part of the second set

collected (up to 23:08 minutes of data).

Images were collected with the following parameters. T1w: matrix size 320x320,

FOV 256x256 mm, 0.8 mm isotropic, flip angle = 8°, TE = 2.24 ms, TR = 2400/1060 ms.

T2w: matrix size 320x320, FOV 256x256 mm, 0.8 mm isotropic, variable flip angle, TE

= 564 ms, TR = 3200 ms. Field maps (PA/AP): matrix size 104x91, FOV 208x208 mm, 2

mm isotropic, flip angle = 90°, TE = 66 ms, TR = 8000 ms. rsfMRI (PA/AP): matrix size

104x91, FOV 208x208 mm, 2 mm isotropic, flip angle = 52°, TE = 37 ms, TR = 800 ms,

time = 5:47.

Preprocessing

Data were organized using the Brain Imaging Data Structure (BIDS, Gorgolewski et al.,

2013) and processed using the publicly available Developmental Cognition and

Neuroimaging (DCAN) lab fMRI Pipeline (Fair et al., 2020). This BIDS application

initiates a functional MRI processing pipeline built upon the Human Connectome

Project's minimal processing pipelines (Glassera et al., 2013). The pipeline comprises six

main stages: 1) PreFreesurfer, 2) FreeSurfer, 3) PostFreesurfer, 4) Volume, 5) Surface,

and 6) DCAN BOLD processing, which is described in depth in Fair et al. (2018). A brief

description of the pipeline follows. PreFreesurfer aligns anatomical data (both T1 and T2)

to the AC-PC axis and then non-linearly normalizes them to an age-specific atlas, and

creates segmentations using joint label fusion (Wang, et al., 2013). FreeSurfer aligns T1

to an atlas using boundary-based registration (Greve & Fischl, 2009) and produces and

refines native cortical surfaces (Fischl, 2012), using intensity adjustments on each ROI separately. PostFreeSurfer converts the FreeSurfer outputs to CIFTI space. The Volume and Surface steps preprocess and align BOLD data to CIFTI space. The average volume was calculated from rigid-body alignment and registered to the T1. BOLD data were then projected onto the surface representation of the cortical ribbon, and down-sampled to the standard surface space and smoothed using a 2mm full-width-half-max Gaussian filter. Finally, the DCAN BOLD connectivity processing stream (Miranda-Dominguez et al., 2020) reduces spurious variance, by regressing averaged grey matter signal, and white matter and ventricular regions. Data were filtered using a bandstop filter of (16.8896, 28.6662) Hz across all participants. Framewise displacement and other movement metrics are calculated, but poor frames are treated later in analysis.

Definition of ROIs and Functional Connectivity Computation

ROIs (n=230) were adopted from previous work examining functional connectivity in infants (Pruett et al., 2015), and projected to a surface representation for cortical ROIs, using 10 mm-diameter spherical representations in volume space. They were a subset of cortical functional areal parcellations obtained in healthy adults (Power et al., 2011) that were found to be stable in gray-matter coverage at different stages in infancy (for more information see Eggebrecht et al., 2017). ROI time series were calculated as the mean across all vertices in the surface representation or across all included voxels in the subcortical ROIs. Pairwise Pearson correlation values were generated for each of the 26,335 possible pairs of ROIs and then Fisher-z transformed.

ROIs were then assigned to functional brain networks based on a network model

derived using the Infomap algorithm (Rosvall & Bergstrom, 2008) on RS data collected

from a different sample of infants (Eggebrecht et al., 2017). Broadly, a correlation matrix

averaged across the sample was binarized at different correlation thresholds (ranging

from 1% to 10% of all possible connections surviving the threshold) to create matrices

with different levels of sparseness. The Infomap algorithm then assigned ROIs to

subnetworks at each correlation matrix based on the maximization of within-module

random walks. Solutions across all the thresholds were combined using an "algorithmic

consensus" procedure. Subnetworks with ≤ 5 ROIs were designed as "Unassigned." This

model summarizes the functional connectivity in the infant-toddler brain into 13 putative

networks (naming informed by adult set of networks): Vis (visual), tDMN (temporal

default mode network), pcDMN (posterior cingulate DMN), aDMN (anterior DMN),

SMN (somato-motor network), SMN2 (somato-motor network 2), DAN (dorsal attention

network), pFPC (posterior frontal parietal control network), aFPC (anterior frontal

parietal control network), SubCtx (subcortex), CO (cingulo-opercular), pCO (posterior

CO), and Sal (salience).

A benefit of using a network solution generated with an independent sample is

that is prevents overfitting. To ensure that this model fit the data from the current sample,

a modularity score (Newman, 2004) was calculated. This score provides a summary of

community structure, or the extent to which ROI-ROI connections within a network are

dense while ROI-ROI connections between networks are sparse. Newman's Qn

calculated at 2.5% edge density was 0.62 in the present sample, indicating that this

network solution had adequate fit for the current sample (for comparison, past work that calculated Newman's Qn in adult resting state networks reported modularity values ranging from roughly 0.5-0.7 (Gordon et al., 2017).

Within-network functional connectivity was calculated by taking the average FC values from all ROIs in the network. Between-network functional connectivity was calculated by taking the average pair-wise correlations between the ROIs in each network. Distributions of the mean within-network functional connectivity values can be seen in Figure 24, and the Infomap-sorted mean functional connectivity MRI matrix derived from the 230 ROIs can be seen in Figure 25.
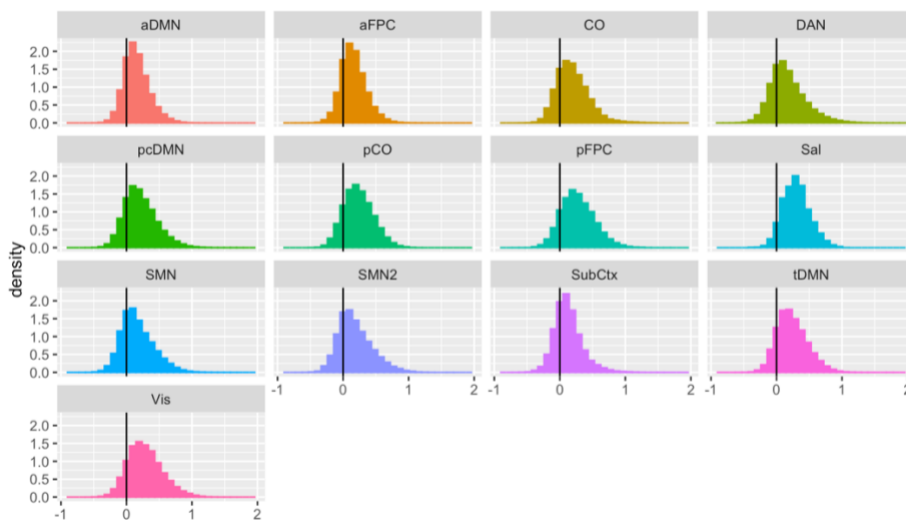

Figure 24. Z-score distributions of participants' within-network connectivity values for each network.
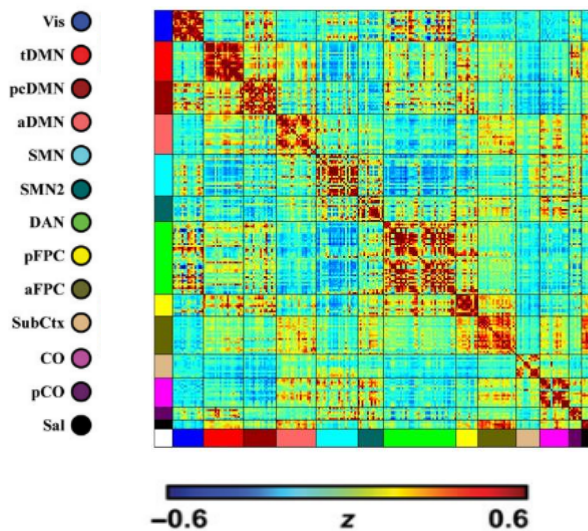
Figure 25. Info-map sorted functional connectivity matrix.

Networks of interest

The present study used pre-defined network assignments, as described in the previous

section. One challenge in generating hypotheses about specific networks is that there are

inconsistencies in how networks are defined (Uddin, Thomas Yeo, & Spreng, 2019). In

the present study, the salience (SAL) and cingulo-opercular (CO) networks contain ROIs

associated with the ventral stream (e.g., IFG, superior temporal sulcus inferior parietal

lobule, see Table 6). Given that only 5 ROIs were assigned to the SAL network (all in

regions with the Talairach label IFG), mean connectivity across the SAL and CO

networks will be calculated and used for analyses as "ventral attention areas." All ROIs

from the DMN sub-networks (aDMN, pcDMN, tDMN) were used for calculating within-

network FC in the DMN, and DMN-DAN between-network connectivity.

Network	Sub-networks	Talairach Label	Number of included ROIs
Cingulo-opercular	**CO**	Cerebellum, insula, auditory cortex, superior temporal sulcus, postcentral gyrus, precentral gyrus.	16
	Posterior CO	Auditory cortex, inferior parietal lobule, insula, postcentral gyrus. Posterior cingulate, superior temporal gyrus.	7
Salience		IFG	5
Dorsal Attention Network		Cerebellum, Fusiform, vWFA, inferior occipital gyrus, inferior parietal, inferior temporal gyrus, lateral occipital gyrus, middle occipital gyrus, middle temporal gyrus, occipital cortex, superior parietal	40
Default Mode Network	**Anterior DMN**	cingulate, IFG, insula, medial frontal gyrus, mFC, middle frontal gyrus, superior frontal cortex	22
	Posterior cingulate DMN	angular gyrus, fusiform gyrus, lateral occipital/parietal cortex, middle occipital gyrus, middle temporal gyrus, parahippocampal gyrus, posterior cingulate, precuneus	18
	Temporal DMN	inferior temp gyrus, middle temporal gyrus, superior temporal gyrus, posterior cingulate, SMG/inferior parietal, inferior parietal	22
Frontoparietal Control Network	**aFPC**	Inferior frontal gyrus, medial frontal gyrus, orbital gyrus, precentral gyrus, superior frontal cortex,	21
	pFPC	angular gyrus, inferior parietal, inferior temporal gyrus, lateral occipital cortex, middle temp gyrus, precuneus	12

Table 6. Each network of interest, and the Talairach labels of the ROIs assigned to those networks.

Aim 1: Model growth in within-network functional connectivity

Analytic plan

Within-network connectivity was calculated for each infant at each time point by averaging across the FC values of each ROI assigned to a given network. Given the accelerated longitudinal design, fixed-effects (e.g. group-level effects) of growth were modelled based on data from cohorts with overlapping age-spans. Random effects of intercept (e.g. individual differences in mean FC values were also estimated. To distinguish between-person effects of age from within-person effects of age, two age

variables were tested in the model: between-person age (age at time of scan, centered on the grand mean) and within-person age (between-person age, centered on the individual's average age across their visits). Subject-level covariates included scanner and sex. Visit-level covariates included motion (remaining mean-wise frame displacement), and the number of attempted resting state runs.

Predictions

Past work has shown positive linear growth in most resting state networks, with the exception of the sensorimotor network which shows declining connectivity over the first two years of life (Gao, Alcauter, Elton, et al., 2015; Gao, Alcauter, Smith, et al., 2015). This work has highlighted more early rapid growth in lower-level networks (e.g. visual networks) than higher-order networks (e.g. DMN, FPC, etc.). I anticipate that the BCP data will replicate these findings in the data covering the first two years of life. Furthermore, it is likely that we will see non-linear growth, such that growth levels off between 2-5 years of age.

Aim 2: Examine relationship between system dynamics of visual attention and resting state network development

Analytic plan

Summarizing eye-tracking measures within a visit

As described in Study 1, α and MF spectrum width are calculated for each time series. Each visit contains three conditions (Social, Pixelated, Attention cue), all of which are comprised of multiple time series. For the hypotheses about DAN-DMN connectivity, I

generated a visit-level summary score for eye-gaze, by taking the average α and tallying

the t-statistic counts (non-significant monofractal, multifractal positive, multifractal

negative) across the entire visit (yielding 4 measures per visit). For the hypotheses about

Sal/CO-FPC connectivity which were specific to stimulus Conditions, I generated these

same summary metrics separately for the Social and Pixelated trials (yielding 8 measures

per visit). The available sample with concurrent MRI and eye-tracking data can be seen

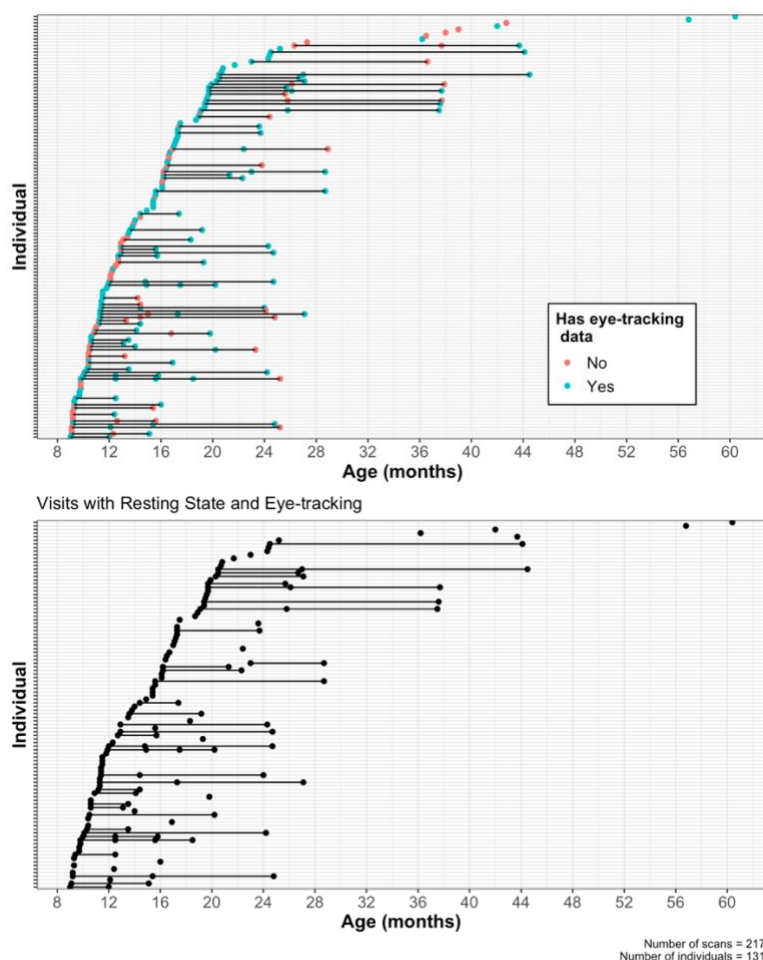in Figure 26, and more data will be added this summer.

Figure 26. Longitudinal data included in sample.
Top figure shows number of MRI visits with resting state, colored by whether there is concurrent eye-tracking data. Bottom figure shows number of MRI visits with both resting state and eye-tracking data. Both figures reflects counts as of March 2021.

Modeling relationship between DAN-DMN connectivity and eye-gaze fractality

First, I will model the longitudinal trajectory of DAN-DMN connectivity to verify that these become more negatively correlated over developmental time in the current sample. Then I will use the mean between-network connectivity scores at each visit as the independent variable, and the tallies of each kind of t-statistic as the dependent variable. Visit-level quality control covariates for eye-tracking (e.g. calibration precision, proportion interpolated) and MRI (e.g. number of resting state runs, remaining mean frame displacement) will be included. To test the specificity of this relationship, in addition to using DAN-DMN connectivity (predictor of interest), I will also model the relationship between eye-gaze fractality and somatomotor-DMN connectivity as I do not predict that there should be significant relationship between these two variables. The predicted results are plotted in Figure 27. Controlling for age, DAN-DMN connectivity – but *not* SMN-DMN connectivity – will be negatively correlated with the number of positive t-statistics in the concurrent eye-tracking. In other words, more negative connectivity between the DAN and DMN networks will predict more nonlinear interactivity that constrains eye-tracking variability. If I find this result, this would suggest that the relationship between DAN-DMN connectivity and behavior observed in adults (Clare Kelly et al., 2008) emerges in infancy as infants become more "adult like" in their functional brain network organization. If I do not find this result, then it is possible that either this brain-behavior relationship does not emerge until later in life, or that there is a lack of within-person stability in these measures that makes it challenging to correlate RS data with behavioral outcomes in infancy.

Modeling relationship between ventral frontoparietal network and eye-gaze fractality

I will use the same approach as above, except the predictor of interest will be mean connectivity between the FPC and Salience/CO networks. Additionally, I will include an interaction term between FC and Stimulus Condition (Social, Pixelated), to test my prediction that the association between FC and eye-gaze will be stronger for data collected in the Social condition.

If I find this Condition-specific effect, this would bolster current theories that visual information from the ventral stream of attention catalyzes the development of frontal areas, serving as one mechanism for experience-dependent individual differences in visual attention (Rosen et al., 2019). If there is a relationship between FC and eye-gaze that is *not* condition specific (e.g. a main effect of FPC-SAL/CO connectivity, but no significant interaction with Condition), then this would suggest that the ventral frontoparietal network may support more domain general attention development.
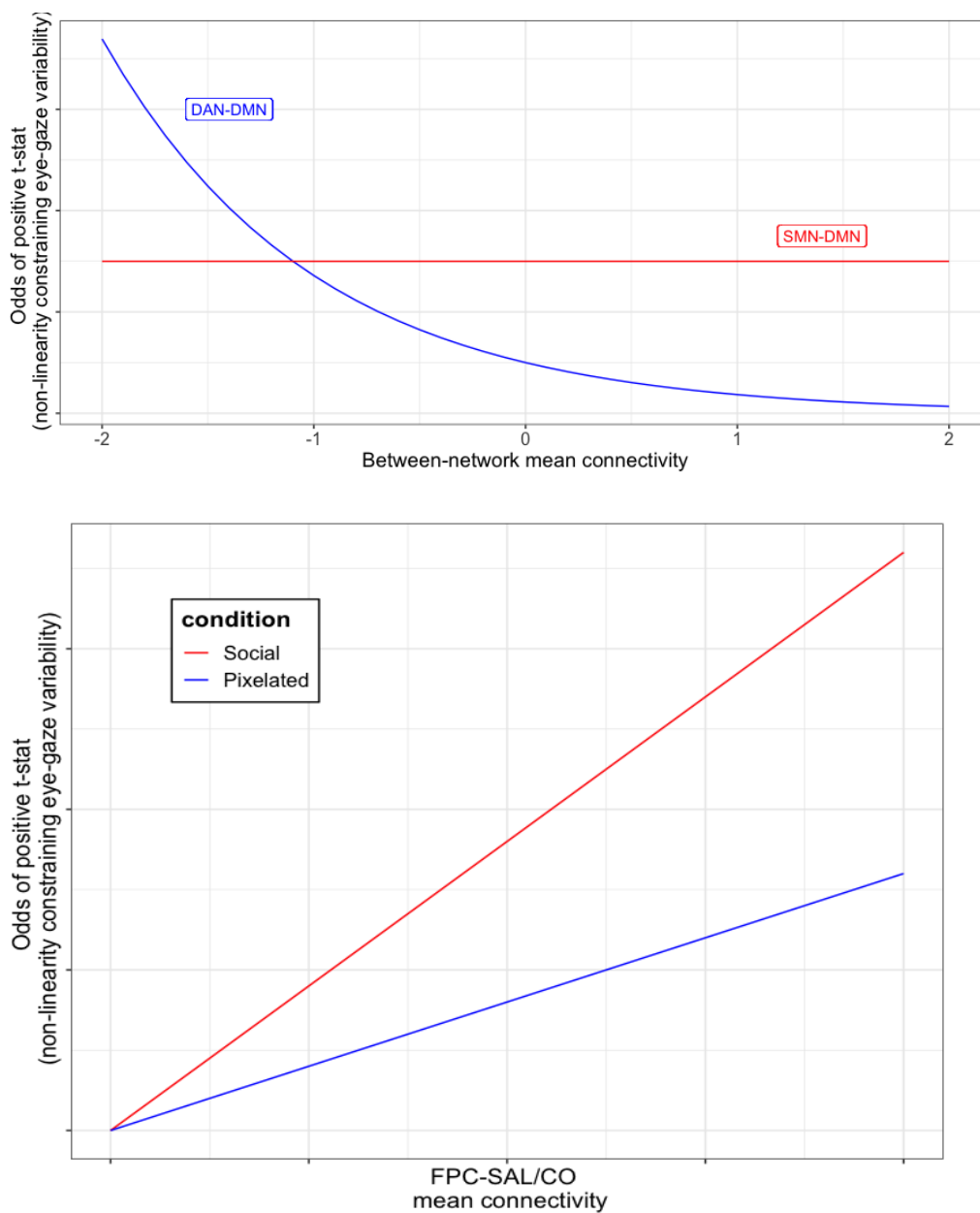
Figure 27. Predicted model results for Aim 2.
Top: More negative DAN-DMN connectivity will be associated with more time series with positive t-statistics, reflecting nonlinear interactivity that constraints system variability. Bottom: Increased positive FPC-SAL/CO connectivity will be associated with more time series with positive t-statistics, particularly in the Social condition.

Summary & Conclusions

This research takes a systems-level approach, applying methods from Complexity Science to understand how infant attention becomes increasingly self-organized in the first years of life. Results provided evidence of self-organization in infants' eye-gaze dynamics as they free-viewed movies, which increased in the first years of life. Findings also suggest that the social content available to the infant via the movies themselves, as well as via infants' spontaneous fixations on areas of the screen with more salient social information, elicited more self-organized eye-gaze dynamics. Results also provided evidence for a more complex form of cross-scale interactivity, as measured by multi-fractal spectrum width. Developmentally, infants' eye-gaze dynamics were more likely to display evidence of cross-scale interactivity that constrains variability in system dynamics as they got older, and when they were presented with social content. In other words, interactions across time scales in infants' attention systems appear to hone attention dynamics, rather than increase randomness. Future work should investigate the relationship between these different categories of multi-fractal systems and metrics like entropy to strengthen this inference.

The next avenue for this research is to examine how brain development supports the coordination of these processes that are critical for visual exploration in infancy (as described in Study 2). An important component of this work will be to first establish whether there is a trait-like complexity "signature" that distinguishes individuals, given the context-dependent nature of these metrics. Overall, intercept-only mixed-effect

models indicated that 23% of variability in α was at the visit-level, and 11.6% was at the

infant-level (collapsed across all of their visits). Identifying the optimal way to quantify a

trait-like "fractal thumbprint" will be critical in order to establish reliable patterns

between eye-gaze dynamics and functional brain development.

References

Aks, D. J., Zelinsky, G., & Sprott, J. C. (2002). Memory across eye-movements: 1/f Dynamic in visual search. *Journal of Vision*, *1*(3), 230–230. https://doi.org/10.1167/1.3.230

Amor, T. A., Reis, S. D. S., Campos, D., Herrmann, H. J., & Andrade, J. S. (2016). Persistence in eye movement during visual search. *Scientific Reports*, *6*, 1–12. https://doi.org/10.1038/srep20815

Amso, D., & Scerif, G. (2015). The attentive brain: insights from developmental cognitive neuroscience. *Nature Reviews Neuroscience*, *16*(10), 606–619. https://doi.org/10.1038/nrn4025

Aslin, R. N. (2007). What's in a look? *Developmental Science*, *10*(1), 48–53.

Bak, P., & Chen, K. (1991). Self-Organized Criticality. *Scientific American*, *264*(1), 46–53.

Bardi, L., Regolin, L., & Simion, F. (2011). Biological motion preference in humans at birth: Role of dynamic and configural properties. *Developmental Science*, *14*(2), 353–359. https://doi.org/10.1111/j.1467-7687.2010.00985.x

Bardi, L., Regolin, L., & Simion, F. (2014). The first time ever I saw your feet: Inversion effect in newborns' sensitivity to biological motion. *Developmental Psychology*, *50*(4), 986–993. https://doi.org/10.1037/a0034678

Bradski, G., & Kaehler, A. (2008). *Learning OpenCV: Computer vision with the OpenCV library.* O'Reilly Media Inc.

Castellanos, F. X., Margulies, D. S., Kelly, A. M. C., Uddin, L. Q., Ghaffari, M., Kirsch, A., … Milham, M. P. (2008). Cingulate - Precuneus Interactions: A New Locus of Dysfunction in Adult Attention-Deficit/Hyperactivity Disorder. *Biological Psychiatry*, *63*(3), 332–337. https://doi.org/10.1016/j.biopsych.2007.06.025.Cingulate

Chhabra, A., & Jensen, R. V. (1989). Direct determination of the singularity spectrum. *Physical Review Letters*, *62*(12), 1327–1330. https://doi.org/10.1103/PhysRevLett.62.1327

Clare Kelly, A. M., Uddin, L. Q., Biswal, B. B., Castellanos, F. X., & Milham, M. P. (2008). Competition between functional brain networks mediates behavioral variability. *NeuroImage*, *39*(1), 527–537. https://doi.org/10.1016/j.neuroimage.2007.08.008

Coey, C. a., Wallot, S., Richardson, M. J., & Van Orden, G. C. (2012a). On the Structure of Measurement Noise in Eye-Tracking. *Journal of Eye Movement Research*, *5*(4), 1–10. https://doi.org/10.16910/jemr.5.4.5

Coey, C. a., Wallot, S., Richardson, M. J., & Van Orden, G. C. (2012b). On the Structure

of Measurement Noise in Eye-Tracking. *Journal of Eye Movement Research*, *5*(4), 1–10. https://doi.org/10.16910/jemr.5.4.5

Corbetta, M., Kincade, J. M., Ollinger, J. M., McAvoy, M. P., & Shulman, G. L. (2000). Erratum: Voluntary orienting is dissociated from target detection in human posterior parietal cortex (Nature Neuroscience (2000) 3 (292-297)). *Nature Neuroscience*, *3*(5), 521. https://doi.org/10.1038/74905

Corbetta, Maurizio, Patel, G., & Shulman, G. L. (2008). The Reorienting System of the Human Brain: From Environment to Theory of Mind. *Neuron*, *58*(3), 306–324. https://doi.org/10.1016/j.neuron.2008.04.017

Desimone, R., & Duncan, J. (1995). Neural Mechanisms of Selective visual attention. *Annual Review of Neuroscience*, *18*, 193–222. https://doi.org/10.4135/9781483328768.n2

Dosenbach, N. U. F., Koller, J. M., Earl, E. A., Miranda-Dominguez, O., Klein, R. L., Van, A. N., Snyder, A. Z., Nagel, B. J., Nigg, J. T., & Nguyen, A. L., Wesevich, V., Greene, D. J., & Fair, D. A. (2017). Real-time motion analytics during brain MRI improve data quality and reduce costs. *Neuroimage*, *161*.

Downey, A. B. (2012). Think Complexity. *Green Tea Press*, 160. https://doi.org/10.1017/CBO9781107415324.004

Eddy, C. L., & Kelty-Stephen, D. G. (2015). Nesting of Focal Within Peripheral Vision Promotes Interactions Across Nested Time Scales in Head Sway: Multifractal Evidence From Accelerometry During Manual and Walking-Based Fitts Tasks. *Ecological Psychology*. Taylor & Francis. https://doi.org/10.1080/10407413.2015.991663

Eggebrecht, A. T., Elison, J. T., Feczko, E., Todorov, A., Wolff, J. J., Kandala, S., … Pruett, J. R. (2017). Joint Attention and Brain Functional Connectivity in Infants and Toddlers. *Cerebral Cortex*, *27*(3), 1709–1720. https://doi.org/10.1093/cercor/bhw403

Fair, D. A., Miranda-Dominguez, O., Snyder, A. Z., Perrone, A., Earl, E. A., Van, A. N., ... & Dosenbach, N. U. (2020). Correction of respiratory artifacts in MRI head motion estimates. *Neuroimage*.

Fair, D. A., Cohen, A. L., Dosenbach, N. U. F., Church, J. A., Miezin, F. M., Barch, D. M., … Schlaggar, B. L. (2008). The maturing architecture of the brain's default network. *Proceedings of the National Academy of Sciences of the United States of America*, *105*(10), 4028–4032. https://doi.org/10.1073/pnas.0800376105

Fair, D. A., Posner, J., Nagel, B. J., Bathula, D., Costa-Dias, T. G., Mills, K. L., … Joel, T. (2010). Atypical Default Network Connectivity in Youth with ADHD. *Biological Psychiatry*, *68*(12), 1084–1091. https://doi.org/10.1016/j.biopsych.2010.07.003.Atypical

Farroni, T., Csibra, G., Simion, F., & Johnson, M. H. (2002). Eye contact detection in

humans from birth. *Proceedings of the National Academy of Sciences of the United States of America*, *99*(14), 9602–9606. https://doi.org/10.1073/pnas.152159999

Fischl, B. (2012). FreeSurfer. *NeuroImage*, *62*.

Frank, M. C., Vul, E., & Johnson, S. P. (2009). Development of infants' attention to faces during the first year. *Cognition*, *110*(2), 160–170. https://doi.org/10.1016/j.cognition.2008.11.010

Frank, M. C., Vul, E., & Saxe, R. (2012). Measuring the Development of Social Attention Using Free-Viewing. *Infancy*, *17*(4), 355–375. https://doi.org/10.1111/j.1532-7078.2011.00086.x

Gao, W., Alcauter, S., Elton, A., Hernandez-Castillo, C. R., Smith, J. K., Ramirez, J., & Lin, W. (2014). Functional Network Development During the First Year: Relative Sequence and Socioeconomic Correlations. *Cerebral Cortex*, (September), 1–10. https://doi.org/10.1093/cercor/bhu088

Gao, W., Alcauter, S., Elton, A., Hernandez-Castillo, C. R., Smith, J. K., Ramirez, J., & Lin, W. (2015). Functional network development during the first year: Relative sequence and socioeconomic correlations. *Cerebral Cortex*, *25*(9), 2919–2928. https://doi.org/10.1093/cercor/bhu088

Gao, W., Alcauter, S., Smith, J. K., Gilmore, J. H., & Lin, W. (2015). Development of human brain cortical network architecture during infancy. *Brain Structure and Function*, *220*(2), 1173–1186. https://doi.org/10.1007/s00429-014-0710-3

Gao, W., Gilmore, J. H., Giovanello, K. S., Smith, J. K., Shen, D., Zhu, H., & Lin, W. (2011). Temporal and spatial evolution of brain network topology during the first two years of life. *PLoS ONE*, *6*(9). https://doi.org/10.1371/journal.pone.0025278

Gao, W., Gilmore, J. H., Shen, D., Smith, J. K., Zhu, H., & Lin, W. (2012). The synchronization within and interaction between the default and dorsal attention networks in early infancy. *Cerebral Cortex*, *23*(3), 594–603. https://doi.org/10.1093/cercor/bhs043

Gao, W., Zhu, H., Giovanello, K. S., Smith, J. K., Shen, D., Gilmore, J. H., & Lin, W. (2009). Evidence on the emergence of the brain's default network from 2-week-old to 2-year-old healthy pediatric subjects. *Proceedings of the National Academy of Sciences of the United States of America*, *106*(16), 6790–6795. https://doi.org/10.1073/pnas.0811221106

Gibson, E., & Pick, A. (2000). An Ecological Approach to Perceptual Learning and Development. *An Ecological Approach to Perceptual Learning and Development*. Retrieved from http://books.google.com/books?hl=en&lr=&id=8LfPKYbWhqoC&oi=fnd&pg=PA3&dq=An+ecological+approach+to+perceptual+learning+and+development&ots=QEtCArQAGQ&sig=kxP0hIRcnEObk69DBHneCMrrzPU

Gilden, D. L. (2001). Cognitive Emissions of 1 / f Noise, *108*(1), 33–56.

Gordon, E. M., Laumann, T. O., Gilmore, A. W., Newbold, D. J., Greene, D. J., Berg, J. J., … Dosenbach, N. U. F. (2017). Precision Functional Mapping of Individual Human Brains. *Neuron*, *95*(4), 791-807.e7. https://doi.org/10.1016/j.neuron.2017.07.011

Gorgolewski, K. J., Alfaro-Almagro, F., Auer, T., Bellec, P., Capotă, M., Chakravarty, M. M., ... & Poldrack, R. A. (2013). BIDS apps: Improving ease of use, accessibility, and reproducibility of neuroimaging data analysis methods. *PLoS Computational Biology*, *13*.

Greve, D. N., & Fischl, B. (2009). Accurate and robust brain image alignment using boundary-based registration. *NeuroImage*, *48*.

Hershman, R., Henik, A., & Cohen, N. (2018). A novel blink detection method based on pupillometry noise. *Behavior Research Methods*, *50*(1), 107–114. https://doi.org/10.3758/s13428-017-1008-1

Hessels, R. S., & Hooge, I. T. C. (2019). Eye tracking in developmental cognitive neuroscience – The good, the bad and the ugly. *Developmental Cognitive Neuroscience*, *40*(July). https://doi.org/10.1016/j.dcn.2019.100710

Hessels, R. S., Niehorster, D. C., Nyström, M., Andersson, R., & Hooge, I. T. C. (2018). Is the eye-movement field confused about fixations and saccades? A survey among 124 researchers. *Royal Society Open Science*, *5*(8). https://doi.org/10.1098/rsos.180502

Howell, B. R., Styner, M. A., Gao, W., Yap, P. T., Wang, L., Baluyot, K., … Elison, J. T. (2019). The UNC/UMN Baby Connectome Project (BCP): An overview of the study design and protocol development. *NeuroImage*, *185*(March 2018), 891–905. https://doi.org/10.1016/j.neuroimage.2018.03.049

Ihlen, E. A. F. (2012). Introduction to multifractal detrended fluctuation analysis in Matlab. *Frontiers in Physiology*, *3 JUN*(June), 1–18. https://doi.org/10.3389/fphys.2012.00141

Ihlen, E. A. F., & Vereijken, B. (2010). Interaction-Dominant Dynamics in Human Cognition : Beyond 1 / f Fluctuation. *Journal of Experimental Psychology. General*, *139*(3), 436–463. https://doi.org/10.1037/a0019098

Itti, L., Koch, C., & Niebur, E. (1998). Short Papers. *Current*, *46*(6), 883–885. https://doi.org/978 0 7340 3893 7

Johnson, M. H. (2005). Subcortical face processing. *Nature Reviews Neuroscience*, *6*(10), 766–774. https://doi.org/10.1038/nrn1766

Kelty-Stephen, D. G. (2018). Multifractal evidence of nonlinear interactions stabilizing posture for phasmids in windy conditions: A reanalysis of insect postural-sway data. *PLoS ONE*, *13*(8), 1–21. https://doi.org/10.1371/journal.pone.0202367

Kelty-Stephen, D. G., & Mirman, D. (2013). Gaze fluctuations are not additively decomposable: Reply to Bogartz and Staub. *Cognition*, *126*(1), 128–134. https://doi.org/10.1016/j.cognition.2012.09.002

Kelty-Stephen, D. G., Palatinus, K., Saltzman, E., & Dixon, J. A. (2013). A Tutorial on Multifractality, Cascades, and Interactivity for Empirical Time Series in Ecological Science. *Ecological Psychology*, *25*(1), 1–62. https://doi.org/10.1080/10407413.2013.753804

Kelty-Stephen, D. G., Stirling, L. A., & Lipsitz, L. A. (2016). Multifractal temporal correlations in circle-tracing behaviors are associated with the executive function of rule-switching assessed by the Trail Making Test. *Psychological Assessment*, *28*(2), 171–180. https://doi.org/10.1037/pas0000177

Klin, A., Shultz, S., & Jones, W. (2015). Social visual engagement in infants and toddlers with autism: Early developmental transitions and a model of pathogenesis. *Neuroscience & Biobehavioral Reviews*, *March*, 189–203. https://doi.org/10.1016/S2215-0366(16)30284-X.Epidemiology

Lee, J. T., & Kelty-Stephen, D. G. (2017). Cascade-driven series with narrower multifractal spectra than their surrogates: Standard deviation of multipliers changes interactions across scales. *Complexity*, *2017*, 16–19. https://doi.org/10.1155/2017/7015243

Lin, W., Zhu, Q., Gao, W., Chen, Y., Toh, C. H., Styner, M., … Gilmore, J. H. (2008). Functional connectivity MR imaging reveals cortical functional connectivity in the developing brain. *American Journal of Neuroradiology*, *29*(10), 1883–1889. https://doi.org/10.3174/ajnr.A1256

Lorenzi, E., Mayer, U., Rosa-Salva, O., & Vallortigara, G. (2017). Dynamic features of animate motion activate septal and preoptic areas in visually naïve chicks (Gallus gallus). *Neuroscience*, *354*, 54–68. https://doi.org/10.1016/j.neuroscience.2017.04.022

Mandelbrot, B. B. (1982). *The Fractal Geometry of Nature*. Times Books.

Markant, J., & Amso, D. (2013). Selective memories: infants' encoding is enhanced in selection via suppression. *Developmental Science*, *16*(6), 926–940. https://doi.org/10.1111/desc.12084

Marlow, C. A., Viskontas, I. V., Matlin, A., Boydston, C., Boxer, A., Taylor, R. P., & Malo, J. (2015). Temporal structure of human gaze dynamics is invariant during free viewing. *PLoS ONE*, *10*(9), 1–13. https://doi.org/10.1371/journal.pone.0139379

Matthew F. Glassera, Stamatios N Sotiropoulosb, J Anthony Wilsonc, Timothy S Coalsona, Bruce Fischld, e, Jesper L Anderssonb, Junqian Xuf, g, Saad Jbabdib, Matthew Websterb, Jonathan R Polimenid, David C Van Essena, Mark Jenkinsonb, and for the W.-M. H. C., & Stamatios. (2013). The Minimal Preprocessing Pipelines for the Human Connectome Project Matthew. *Neuroimage*. https://doi.org/10.1016/j.neuroimage.2013.04.127.The

Newman, M. E. J. (2004). Fast algorithm for detecting community structure in networks. *Physical Review E - Statistical Physics, Plasmas, Fluids, and Related Interdisciplinary Topics*, *69*(6), 5. https://doi.org/10.1103/PhysRevE.69.066133

Power, J. D., Cohen, A. L., Nelson, S. M., Wig, G. S., Barnes, K. A., Church, J. A., … Petersen, S. E. (2011). Functional Network Organization of the Human Brain. *Neuron*, *72*(4), 665–678. https://doi.org/10.1016/j.neuron.2011.09.006

Pruett, J. R., Kandala, S., Hoertel, S., Snyder, A. Z., Elison, J. T., Nishino, T., … Piven, J. (2015). Accurate age classification of 6 and 12 month-old infants based on resting-state functional connectivity magnetic resonance imaging data. *Developmental Cognitive Neuroscience*, *12*, 123–133. https://doi.org/10.1016/j.dcn.2015.01.003

Rosen, M. L., Amso, D., & McLaughlin, K. A. (2019). The role of the visual association cortex in scaffolding prefrontal cortex development: A novel mechanism linking socioeconomic status and executive function. *Developmental Cognitive Neuroscience*, *39*(July), 100699. https://doi.org/10.1016/j.dcn.2019.100699

Rosvall, M., & Bergstrom, C. T. (2008). Maps of random walks on complex networks reveal community structure. *Proceedings of the National Academy of Sciences of the United States of America*, *105*(4), 1118–1123. https://doi.org/10.1073/pnas.0706851105

Schreiber, T., & Schmitz, A. (1996). Improved Surrogate Data for Nonlinearity Tests. *Physical Review Letters*, *77*(4), 635–638.

Stallworthy, I. C., Sifre, R., Berry, D., Lasch, C., Smith, T. J., & Elison, J. T. (2020). Infants' gaze exhibits a fractal structure that varies by age and stimulus salience. *Scientific Reports*, *10*(1), 1–14. https://doi.org/10.1038/s41598-020-73187-w

Stan, C., Astefanoaei, C., Pretegiani, E., Optican, L., Creanga, D., Rufa, A., & Critescu, C. (2014). Nonlinear analysis of saccade speed fluctuations during combined action and perception tasks. *J Neuroscience Methods*, *232*. https://doi.org/10.1016/j.jneumeth.2014.05.010.Nonlinear

Stephen, D. G., & Anastas, J. (2011). Fractal fluctuations in gaze speed visual search. *Attention, Perception, and Psychophysics*, *73*(3), 666–677. https://doi.org/10.3758/s13414-010-0069-3

Stephen, D. G., & Mirman, D. (2010). Interactions dominate the dynamics of visual cognition. *Cognition*, *115*(1), 154–165. https://doi.org/10.1016/j.cognition.2009.12.010

Stephen, D. G., Mirman, D., Magnuson, J. S., & Dixon, J. A. (2009). Lévy-like diffusion in eye movements during spoken-language comprehension. *Physical Review E - Statistical, Nonlinear, and Soft Matter Physics*, *79*(5), 1–6. https://doi.org/10.1103/PhysRevE.79.056114

Uddin, L. Q., Thomas Yeo, B. T., & Spreng, R. N. (2019). Towards a universal

taxonomy of macro-scale functional human brain networks. *Brain Topography*, *32*(6). https://doi.org/10.1007/s10548-019-00744-6.Towards

Valenza, E., Simion, F., Cassia, V. M., & Umiltà, C. (1996). Face preference at birth. *Journal of Experimental Psychology: Human Perception and Performance*, *22*(4), 892–903. https://doi.org/10.1037/0096-1523.22.4.892

Van Essen, D. C., Smith, S. M., Barch, D. M., Behrens, T. E. J., Yacoub, E., &, & Ugurbil, K. (2013). The WU-Minn Human Connectome Project: An overview. *NeuroImage*, *80*.

Van Orden, G. C., Holden, J. G., & Turvey, M. T. (2003). Self-organization of cognitive performance. *Journal of Experimental Psychology: General*, *132*(3), 331–350. https://doi.org/10.1037/0096-3445.132.3.331

Van Orden, G. C., Kloos, H., & Wallot, S. (2011). *Living in the Pink. Intentionality, Wellbeing, and Complexity*. *Philosophy of Complex Systems* (Vol. 10). Elsevier B.V. https://doi.org/10.1016/B978-0-444-52076-0.50022-5

Wallot, S., O'Brien, B. A., Haussmann, A., Kloos, H., & Lyby, M. S. (2014). The Role of Reading Time Complexity and Reading Speed in Text Comprehension. *Journal of Experimental Psychology : Learning , Memory , and Cognition*, *40*(6), 1745–1765.

Wang, H., Suh, J. W., Das, S. R., Pluta, J., Craige, C., & Yushkevich, P. A. (2013). Multi-Atlas Segmentation with Joint Label Fusion. *IEEE Transactions on Pattern Analysis and Machine Intelligence*, *35*.

Wang, Q., Kim, E., Chawarska, K., Scassellati, B., Zucker, S., & Shic, F. (2014). On relationships between fixation identification algorithms and fractal box counting methods. *Proceedings of the Symposium on Eye Tracking Research and Applications - ETRA '14*, 67–74. https://doi.org/10.1145/2578153.2578161

Wink, A. M., Bullmore, E., Barnes, A., Bernard, F., & Suckling, J. (2008). Monofractal and multifractal dynamics of low frequency endogenous brain oscillations in functional MRI. *Human Brain Mapping*, *29*(7), 791–801. https://doi.org/10.1002/hbm.20593

Zhang, H., Shen, D., & Lin, W. (2019). Resting-state functional MRI studies on infant brains: A decade of gap-filling efforts. *NeuroImage*, *185*(July 2018), 664–684. https://doi.org/10.1016/j.neuroimage.2018.07.004